J Nanopart Res (2026) 28:146
https://doi.org/10.1007/s11051-026-06673-3

RESEARCH

Differential toxicities of manganese ferrite nanoparticles from two synthesis methods using developing zebrafish (*Danio rerio*): towards a biocompatible and safe magnetic nanoparticles

Jaqueline Cardoso Jacintho · Bianca Leite Carnib · Vitória Gabriela Reis de Sousa · Marcus Vinícius Araújo · Andris Figueiroa Bakuzis · Thiago Lopes Rocha

Received: 24 February 2026 / Accepted: 19 May 2026 / Published online: 25 May 2026

Abstract Manganese ferrite nanoparticles ($MnFe_2O_4$ NPs) have several environmental and biomedical applications. However, knowledge about their toxicity, as a function of the synthesis method, is still scarce. Thus, the current study aimed to evaluate whether the synthesis method (hydrothermal: HT NPs; coprecipitation: CP NPs) of citrate-coated $MnFe_2O_4$ NPs influences their potential toxicity in zebrafish embryos and larvae through multiple biomarker assessment. HT NPs were synthesized at high pressure and temperature, whereas CP NPs synthesis included a passivation step. Fe and Mn were detected in zebrafish chorion exposed to the higher concentration of HT and CP NPs, but they were not detected on the larvae's body surface. The $MnFe_2O_4$ NPs did not induce mortality or inhibit hatching. HT NPs (5.0 and 10 mg L^{-1}) and CP NPs (1.25 to 10 mg L^{-1}) reduced the spontaneous contraction frequency in zebrafish embryos. HT NPs (5.0 and 10 mg L^{-1}) induced tachycardia, CP NPs (2.5, 5.0, and 10 mg L^{-1}) induced bradycardia in zebrafish embryos. Pericardial edemas were a transient effect, detected only in embryos exposed to HT NPs for 48 h. After 72 h of exposure, neither NP type induced significant morphological alterations, changes in ROS levels, effects on cell viability, or behavioral alterations. Overall, synthesis-dependent early developmental effects were observed, with no evidence of persistent post-hatching toxicity under the experimental conditions. Thus, the zebrafish is a suitable model system to compare NPs effects from different synthesis methods, contributing to the development of safer nanotechnologies.

Keywords Nanotoxicity · Ferrite nanoparticles · Developmental toxicity · Ecotoxicity · Synthesis

Introduction

Manganese ferrite nanoparticles ($MnFe_2O_4$ NPs) are a type of iron oxide nanoparticles (IONPs) with several biomedical and environmental applications [1]. The similarity to magnetite (Fe_3O_4) arises from the fact that its structure contains Fe^{2+} and Fe^{3+}, while Mn-ferrite NPs contain Mn^{2+} and Fe^{3+}. $MnFe_2O_4$ NPs can be used in magnetic resonance imaging (MRI) as contrast agents [2, 3], delivery of antitumoral drugs [4], photothermal therapy [5, 6], and magnetic

Supplementary Information The online version contains supplementary material available at https://doi.org/10.1007/s11051-026-06673-3.

J. C. Jacintho · B. L. Carnib · V. G. R. de Sousa · T. L. Rocha (✉)
Laboratory of Environmental Biotechnology and Ecotoxicology, Institute of Tropical Pathology and Public Health, Federal University of Goiás, Goiânia, Brazil
e-mail: thiagorochabio20@gmail.com

M. V. Araújo · A. F. Bakuzis
Nanomedicine Integrated Research Center, Institute of Physics, Federal University of Goiás, Goiânia, Brazil

hyperthermia [7]. In addition, $MnFe_2O_4$ NPs can be applied as a Fe and Mn-rich fertilizer in agriculture [8], for enhancing carbon sequestration by microalgae [9], remediation of Cr^{6+} contaminated environments [10], or in the remediation of dye- [11] and gadolinium-contaminated waters [12].

IONPs have been used in the clinic [13] and environmental applications for decades [14], but it is still necessary to determine safe concentration ranges and the potential sublethal effects in non-target organs and species, mainly with distinct ferrites. The toxicity of IONPs has been evaluated by in vitro and in vivo approaches. IONPs have been reported to inhibit the growth of lung cancer cells (NCI-H460 line) [15], and to increase oxidative stress, apoptosis, and myocardial dysfunctions in mice [16], genotoxic and cardiotoxic effects in rats [17], and genotoxic and cardiotoxic effects in the freshwater fish *Poecilia reticulata* [18]. Although there are still gaps between in vitro, ex vivo, and in vivo toxicity tests with IONPs, the teleost zebrafish (*Danio rerio*) emerges as an excellent intermediate model of NPs toxicity tests between the cell culture and mammalian models [19], also avoiding the excessive use of rodents [20].

Approximately 70% of genetic similarity between zebrafish and humans [21] contributes to translational research and facilitates the generation of transgenic lines [22]. The high reproduction rate and small size are features that facilitate care, cultivation, and maintenance of the animals [23]. One of the most important advantages is the optical transparency of embryos and larvae, which enables monitoring of NPs and cancer cells and their effects on zebrafish development [24]. Moreover, the zebrafish embryo-larval toxicity test (ZELT) described by the Organisation for Economic Cooperation and Development (OECD) in the test guideline number 236 [25] contributed to the increasing production of papers applied to nanotoxicological research [26–28].

The toxicity of IONPs in zebrafish depends on diameter, composition, functionalization, concentration, exposure time, developmental stage, and type of exposure [29, 30]. Citrate-functionalized maghemite (γ-Fe_2O_3 NPs) adhered to the zebrafish chorion (after 48 h post-exposure—hpe) and accumulated in the digestive system and liver of zebrafish larvae after 144 hpe [29]. Uncoated maghemite Fe_2O_3 NPs induced oxidative stress and mortality above 20 mg L^{-1} in zebrafish embryos and larvae [31]. Citrate-coated γ-Fe_2O_3 NPs [29] and green Fe_3O_4 NPs synthesized from the extract of *Phyllanthus niruri* [32] also induced bradycardia, pericardial edemas, and blood accumulation in the heart of zebrafish embryos. Besides, chitosan-coated Fe_3O_4 NPs induced behavioral effects, such as thigmotaxis and escape response to an aversive stimulus [30], but no mortality was observed in adult zebrafish after exposure to 75 mg L^{-1} citrate-coated Fe_2O_3 NPs [33]. Also, polyethylene-glycol (PEG)-coated MnFe NPs (3.2 nm) at 100 mg L^{-1} induced higher mortality in zebrafish embryos than PEG-coated Fe NPs (3.5 nm) [20]. On the other hand, zebrafish larvae (96 h) exposed to hybrid manganese oxide (Mn_2O_3)-carboxymethyl cellulose-L-arginine hybrid nanomaterials (Mn_2O_3-CMC-LA HNMs), at 1 mg mL^{-1} with 50–100 nm individual size, had 100% survival [34].

Despite the growing literature on the toxicity of IONPs, knowledge regarding the influence of synthesis methods on toxicity remains limited. For example, green Fe_3O_4 NPs synthesized from the extract of *Withania somnifera*, meso-2,3 dimercaptosuccinic acid (DMSA) coated, presented fewer toxic effects than coprecipitated ones, in zebrafish 96 h exposure [35]. Thus, the present study aimed to evaluate whether the synthesis method of citrate-coated $MnFe_2O_4$ NPs (hydrothermal synthesis: HT NPs, and coprecipitation synthesis: CP NPs), influence their potential toxicity in zebrafish embryos and larvae, using multiple biomarker assessments. The hypothesis that the synthesis method of $MnFe_2O_4$ NPs influences toxicity in developing zebrafish was tested. To the best of our knowledge, this is the first study to focus on investigating the effects of hydrothermal and coprecipitation synthesis methods on the toxicity of $MnFe_2O_4$ NPs in developing zebrafish. This study contributes to the development of safer and more sustainable NPs in the context of human, animal, and environmental health (One Health).

Materials and methods

Nanoparticles

The $MnFe_2O_4$ NPs were obtained via hydrothermal [36] and coprecipitation methods [37]. The hydrothermal synthesis initiated by preparing a mixture

of 10 mL of Fe^{3+} and 5 mL of Mn^{2+} stock solutions ($FeCl_3{\cdot}6H_2O$, $MnCl_2{\cdot}4H_2O$) with 40 mL of methylamine (40 wt % CH_3NH_2), under stirring for 10 min. Then, the material was subjected to high pressure and temperature in a Teflon-sealed autoclave heated up to 160 °C. Further, the precipitate was separated by magnetic decantation, washed with deionized water, and redispersed in 50 mL of ultrapure water. Thus, the citrate coating was performed by adding 4 mmol of $Na_3C_6H_5O_7{\cdot}2H_2O$ to the solution under boiling conditions with continuous stirring. Finally, the pH was adjusted to 7.0, and the precipitate was washed with acetone. The HT NPs were redispersed in 50 mL of ultrapure water, forming the final magnetic fluid [36].

The coprecipitation synthesis involved the addition of 50 mmol of $FeCl_3$ and 25 mmol of $MnCl_2$ (both dissolved in 100 mL of 3% HCl w/w) into 500 mL of boiling 2.0 mol L^{-1} methylamine solution, under stirring for 30 min. The resulting material was magnetically separated from the supernatant and washed with distilled water. The precipitate was acidified with 0.5 mol L^{-1} HNO_3 solution and magnetically separated from the supernatant. Then, 0.5 mol L^{-1} of ferric nitrate $Fe(NO_3)_3$ was added and stirred for 30 min under heating by boiling, which was the passivation step. The precipitate was magnetically separated and redispersed in 50 mL of water for sodium citrate coating, stirring for 30 min (mass ratio of 5% between $Na_3C_6H_5O_7$ and $MnFe_2O_4$). Further, the precipitate was magnetically separated again and washed with acetone three times. Finally, the magnetic colloid was stably dispersed in water under physiological conditions, forming the CP NPs [37].

The individual size of $MnFe_2O_4$ NPs ($n = 200$ particles) was determined by transmission electron microscopy (TEM) with the JEOL microscope (JEM-2100). The minimum and maximum diameters of the NPs were determined using ImageJ software. The chemical composition was analyzed by Energy Dispersive X-ray Spectroscopy (EDS), Thermo Scientific NSS Spectral Imaging. The crystalline structure of NPs was analyzed by X-ray diffraction (XRD). The crystallite mean diameter was calculated using the Halder-Wagner equation from the data obtained from XRD. The hydrodynamic diameter (Hd), the zeta potential (ζ), and the polydispersity index (PdI) of NPs (5 mg L^{-1}) in ultrapure water (UW) and reconstituted water (RW) (ISO 7346/3, 1996 [38]) were determined using the Zetasizer Nano-ZS90 model (Malvern Panalytical). Hd and PdI were analyzed by dynamic light scattering (DLS), and the zeta potential was measured by electrophoretic light scattering (ELS), through different pH (2, 4, 6, 7, 8, 10, and 12). The dispersions were sonicated in an ultrasonic bath for 30 min prior to analysis. The ultrasonication process was used to improve dispersion prior to analysis [39].

Model system

Zebrafish, AB strain, were obtained from the Multi-User Center of Animal Production and Experimentation (CMPEA) at the Institute of Tropical Pathology and Public Health (IPTSP) of the Federal University of Goiás (UFG). The adult zebrafish were maintained in a recirculation system (Altamar Sistemas Aquáticos®) under controlled conditions of temperature (27 ± 0.5 ºC), pH (7.3 ± 0.2), conductivity (250 ± 50 µS), and a 14:10 h light:dark cycle photoperiod. Zebrafish were fed with commercial fish food (Poytara Flakes for Tropical Fishes) and live food (*Artemia* sp.). Experimental methodologies and animal procedures were approved by the Ethics Committee on the Use of Animals (CEUA—UFG, n. 073/22).

Interaction of NPs with the embryo chorion and larval surface

After 48 h and 144 h of exposure to $MnFe_2O_4$ HT NPs and CP NPs (10 mg L^{-1}), zebrafish embryos and larvae ($n = 3$/group) were selected to evaluate the interaction of NPs with the zebrafish chorion and larval body surface [29]. Animals were fixed by immersion in paraformaldehyde (4%) for 4 h, washed in 0.2 M PBS buffer at pH 7.2, dehydrated through increasing ethanol gradient (70 and 100%), and dried with liquid carbon dioxide (CO_2) in a critical-point drier (Autosamdri® 815 A). Dried materials were sputter-coated with gold in a Denton Vacuum Sputter Coater (Denton Vacuum, LLC, Moorestown, NJ, USA), and analyzed using a scanning electron microscope (SEM) (Jeol JSM-6610) coupled with energy dispersive X-ray spectroscopy (EDS) (Thermo Scientific NSS Spectral Imaging). The EDS analysis of the larval surface body included 4 different regions: eye (point 1), heart (point 2), abdomen (point 3), and tail (point 4) [29].

Zebrafish embryo-larval toxicity test (ZELT)

The zebrafish breeding pairs (1 male: 1 female) were placed in commercial tanks (Alesco®). Then, the embryos were collected, and only viable embryos were selected [40]. Then, one embryo (2–4 h post-fertilization—hpf) per well was placed in 24-well microplates (2 mL/well) for the zebrafish embryo-larval toxicity test (ZELT). The exposure was conducted under static conditions, in three replicates of 10 embryos ($n = 30$ embryos per experimental group) for 144 h. The NP dispersion concentrations were 0.6, 1.25, 2.5, 5.0, and 10 mg L^{-1} based on three criteria. First, previous studies of potential effects of IONPs at similar concentrations in zebrafish [29–32]. Second, concentrations used in studies evaluating in vitro antitumoral potential of $MnFe_2O_4$ NPs [4, 41]. Third, environmentally relevant iron concentrations were considered [42, 43]. We chose the static exposure condition considering the deposition of NPs in the environment without medium renewal as a first stage of analysis of toxicity. This approach with previous studies considering the biomedical applications of $MnFe_2O_4$ NPs [24]. In addition, the positive control group was composed of animals exposed to 4 mg L^{-1} 3,4-Dichloroaniline in reconstituted water (according to OECD) [25], and those from the negative control group was maintaining only reconstituted water (294 mg L^{-1} of $CaCl_2.2H_2O$, 123.3 mg L^{-1} of $MgSO_4.7H_2O$, 63 mg L^{-1} of $NaHCO_3$, and 5.5 mg L^{-1} of KCl) according to ISO 7346/3, 1996 [38], and OECD, 2013 [25]. Temperature (26 ± 1 ºC), pH (7.3 ± 0.2), and 14:10 h ligh:dark photoperiod were maintained constant during the bioassay by using a bio-oxygen demand incubator (BOD) (SOLAB SL-224/120).

During the exposure period (144 h), the zebrafish embryos and larvae were observed daily by a stereomicroscope (Stemi 508, Zeiss) connected to an Axiocam 105 color camera capture system and ZEN Software 2.6 blue edition. Survival and hatching rate (%) were assessed daily. Based on Lammer et al. 2009 [44] and OECD, 2013 [25], embryos and larvae exhibiting coagulation, absence of tail detachment, defective somite formation, and absence of heartbeat were considered dead. At 24 h post-exposure, the spontaneous contraction frequency (SCF) was assessed during 60 s, as an indicator of neurodevelopmental effects [45]. At 48 hpe, the heartbeat frequency (beats per minute) was quantified, as an indicator of cardiac function [46]. The percentages of individuals with bradycardia, tachycardia and normal heartbeat were calculated considering the interval between minimum and maximum heartbeats of the NC group. Morphological changes in zebrafish embryos and larvae (pericardial and yolk sac edema, scoliosis, lordosis, deformities, absence or irregular size of eyes) were analyzed according to Pereira et al. (2019) [26].

Reactive oxygen species

After 144 h of exposure, reactive oxygen species (ROS) levels in zebrafish were measured using the fluorescent reagent 2′,7′-dichlorofluorescein diacetate (DCFH-DA) [47, 48]. Zebrafish larvae ($n = 10$ per replicate; $n = 30$ per group) were euthanized by hypothermia and washed twice with cold PBS (pH = 7.4). Then, they were homogenized ($n = 3$ pools with 10 larvae/group) using a micro-homogenizator (JETTA, G13 model) and the homogenate was centrifuged at 12,000 rpm for 30 min at 4 ºC. Then, 20 µL of the supernatant was added to a 96-well plate and incubated at room temperature for 5 min. 100 µL of PBS and 8.3 µL of DCFH-DA stock solution (dissolved in DMSO, 10 mg mL^{-1}) were added to each well, and the plate was incubated for 30 min [49]. Subsequently, the fluorescence intensity was measured in a microplate reader (Molecular Device, M2, Union City, CA, USA) with excitation and emission wavelengths set at 485 and 530 nm, respectively. The fluorescence intensity values were normalized to the total protein levels determined by the Bradford method [50] and expressed as arbitrary units (fluorescence per mg protein).

Cell viability

Cell viability in the zebrafish larvae was analyzed as described by Zhao et al. (2019) [51] with modifications by Qualhato et al. (2024) [52]. After the exposure period (144 h), the zebrafish larvae ($n = 12$ per experimental group) were washed with reconstituted water (ISO 7346/3, 1996, [38]). Then, 1 mL of reconstituted water containing 1 µL of acridine orange (AO) solution (5 mg mL^{-1}) was added to each well, and the plates were incubated for 15 min at 25 ºC in the dark. After incubation, the AO solution was removed, and the larvae were washed with reconstituted water. The larvae

were then observed under a fluorescence microscope with a capture system (Axio Imager 2, capture system: Axiocam 503 colour; Zeiss). The fluorescence emission captured on the filter (503 nm excitation/528 nm emission) [53] and the captured images were then analyzed using ImageJ software (v.1.54). Head and trunk, tail, and the whole larvae were analyzed to identify cell viability in each region. Cell viability was expressed in terms of relative green fluorescence intensity [52].

Behavioral analysis

After the exposure period (144 h), zebrafish larvae were acclimatized at room temperature for 5 min, and then transferred to 12-well microplates (1 larva per well) containing reconstituted water (3 mL per well). The behavioral analysis followed the protocol developed by Pinheiro-da-Silva et al. (2017) [54] and modified by Santos et al. (2024) [55]. The microplate was placed in a mini studio equipped with a webcam (Logitech C922 Pro®) positioned above, and behavior was recorded for 5 min. The video analysis was conducted in the ZebTrack software implemented in MATLAB (MathWorks, Natick, MA). Mean speed (cm/s), maximum speed (cm/s), total distance traveled (cm), time in peripheral area (s), time in central area (s), and total latency time (s) were recorded as behavioral parameters [55].

Statistical analysis

The statistical analyses of embryo-larval toxicity and behavior parameters were performed using R software and the graphs were generated using GraphPad® Prism 8. Data distribution was analyzed using the Shapiro–Wilk test, and homoscedasticity was assessed using Levene's test. Survival curve analyses were conducted by the Log-Rank test, followed by post hoc tests. One-Way ANOVA and post hoc Tukey's test were applied for data with normal distribution and homoscedasticity (protein quantification). Kruskal–Wallis test and post hoc Dunn's test were used for non-parametric data (SCF, heartbeats, morphological alterations, ROS levels, cell viability, and behavioral tests). The significance level was 0.05. The results of HT and CP exposures were compared with their respective negative control group (NC).

The principal component analysis (PCA) was performed to explore multivariate patterns and identify associations among biomarkers and exposure groups. Variables included spontaneous contraction frequency (sc), heartbeats (hb), mean velocity (vmed), maximum velocity (vmax), total distance traveled (dt), time in peripherical area (tp), time in central area: area 2 (t2), total latency time (lt), ROS levels (ros), cell viability (head and trunk: cvht; tail: cvt; larvae: cvl), and protein levels by bradford (brad).

Results and discussion

NP characterization

TEM results showed spherical morphology for both HT NPs and CP NPs (Fig. 1A,B). The mean smaller diameter was 8.99 ± 2.73 nm for HT NPs (Fig. 1C) and 6.18 ± 2.29 nm for CP NPs (Fig. 1D). The mean larger diameter was 11.12 ± 3.73 nm for HT NPs (Fig. 1C) and 8.48 ± 3.19 nm for CP NPs (Fig. 1D), indicating significant differences in particle size ($p < 0.01$). These results are consistent with previous studies, such as 12 ± 3 nm of $MnFe_2O_4$ CP NPs [37] and 10 ± 2 nm of $MnFe_2O_4$ HT NPs [36]. The crystallite mean diameter was 19.2 nm for HT NPs and 16.5 nm for CP NPs (Fig. S1). Furthermore, the NP composition of iron (Fe) and manganese (Mn) was confirmed by EDS for both NPs (Fig. 1E,F). The presence of Cu in Fig. 1 E,F is derived from the grids of Cu used in the sample holder. The XRD spectrum confirms a single-phase cubic spinel ferrite crystalline structure for the HT NPs and CP NPs (Fig. 1G,H). HT NPs exhibited higher crystallinity than CP NPs, as expected by the difference in the synthesis method.

The difference in size is also corroborated by the magnetization characterization (Fig. S2). The saturation magnetization of HT NPs was 64.2 emu/g, while for CP NPs the value was 51.8 emu/g. The lower magnetization observed for smaller particles has been reported for Mn-ferrite NPs [56]. The existence of a small coercivity value, $Hc = 4.8$ Oe for HT and 19.4 Oe for CP NPs, indicates the presence of a fraction of the NPs in a blocked magnetic state. A typical magnetization profile was observed for both NP types, confirming the superparamagnetic-like behavior (no hysteresis) (Fig. S2), as reported previously by Cintra et al. (2022) [4].

The hydrodynamic diameter of HT NPs (31.72 ± 3.31 nm) and CP NPs (29.82 ± 1.10 nm) were similar in UW ($p > 0.05$; Table 1). On the

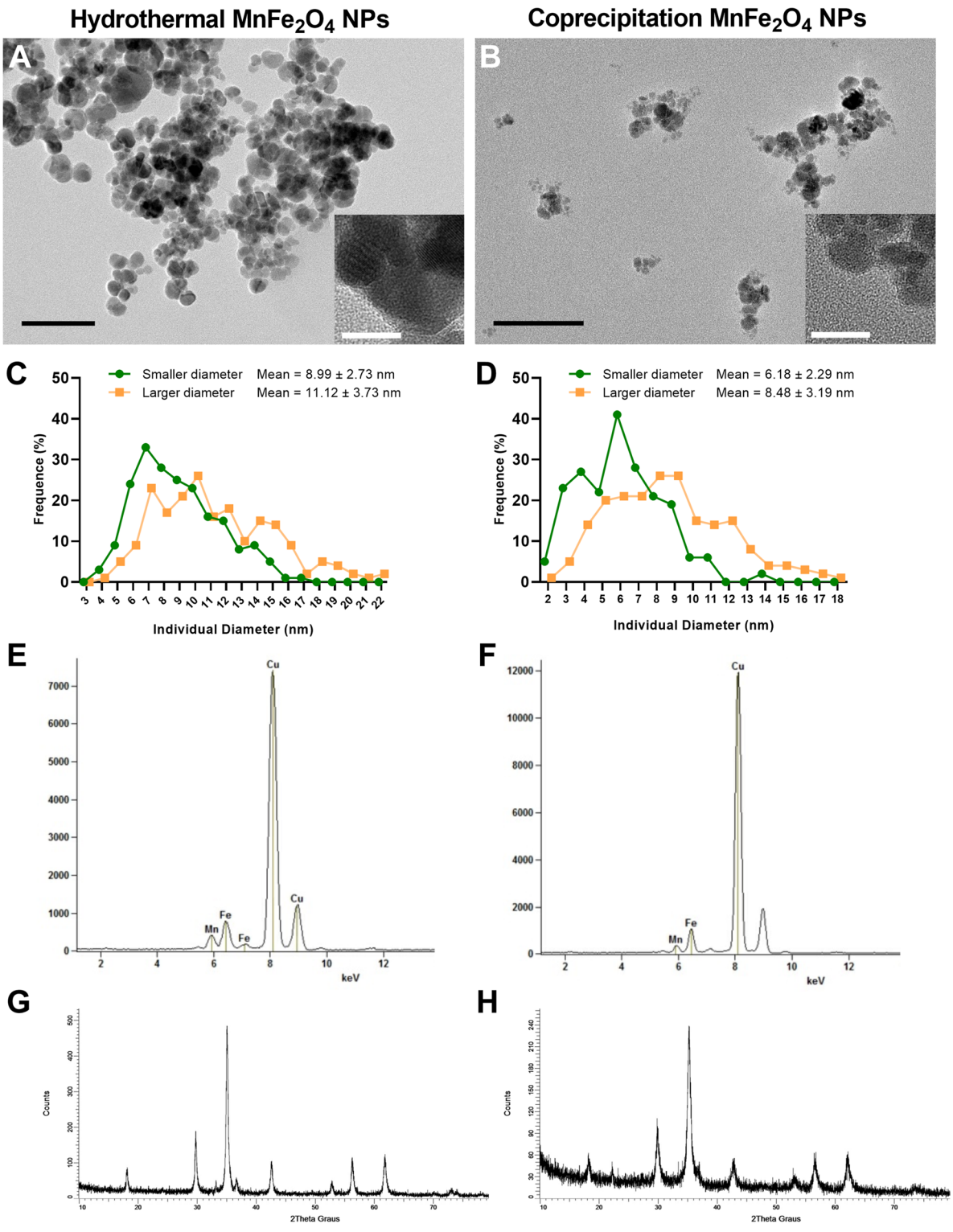
Hydrothermal $MnFe_2O_4$ NPs
Coprecipitation $MnFe_2O_4$ NPs
A
B
C
Smaller diameter Mean = 8.99 ± 2.73 nm
Larger diameter Mean = 11.12 ± 3.73 nm
Frequence (%)
Individual Diameter (nm)
D
Smaller diameter Mean = 6.18 ± 2.29 nm
Larger diameter Mean = 8.48 ± 3.19 nm
Frequence (%)
Individual Diameter (nm)
E
Cu
Fe
Mn
Fe
Cu
keV
F
Cu
Fe
Mn
keV
G
Counts
2Theta Graus
H
Counts
2Theta Graus

◂**Fig. 1** Citrate-coated manganese ferrite nanoparticles ($MnFe_2O_4$ NPs) characterization of hydrothermal (HT NPs) and coprecipitation (CP NPs) synthesis method. Transmission Electronic Microscopy (TEM) of HT NPs **A** and CP NPs **B**, major scale bar: 100 nm and minor scale bar: 20 nm. Individual diameter of HT NPs **C** and CP NPs **D**. Energy Dispersive X-ray Spectroscopy (EDS) of HT NPs **E** and CP NPs **F**. X-ray diffraction (XRD) of HT NPs **G** and CP NPs **H**

other hand, the hydrodynamic diameter of CP NPs (334.07 ± 24.48 nm) were higher than HT NPs (121.05 ± 35.69 nm) in RW, indicating increased agglomeration/aggregation ($p < 0.01$). The zeta potential was negative for both NPs in UW (HT = −27.66 ± 0.36 mV; CP = −28.85 ± 0.55 mV; $p < 0.05$) and RW (HT = −14.74 ± 2.10 mV; CP = −15.88 ± 0.37 mV; $p > 0.05$), consistent with the presence of citrate coating, which confers a negative surface charge to IONPs in RW [29]. Although the zeta potential was close to 30 mV in UW, the value became closer to 0 mV in RW (Table 1), which indicates reduced colloidal stability [57]. In the case of RW, the salts dissociate into ions in the water medium (such as Cl^-, SO_4^{2-}, HCO_3^-, Ca^{2+}, Mg^{2+}, Na^+, and K^+), which form a solvation layer around the NPs, influencing zeta potential and hydrodynamic size [58]. The PdI of both synthesis NPs in UW were smaller than 0.5 ($p > 0.05$), like other citrate-coated $MnFe_2O_4$ NPs [36]. However, in RW, the PdI increased for both NPs ($p > 0.05$), demonstrating increased polydispersity, showing the agglomeration process (Table 1). NPs aggregates/agglomerates can influence the interaction with zebrafish and affect exposure dynamics [59]. The size of NPs may reach the micrometer scale, altering the mode of interaction with the zebrafish chorion; the aggregation/agglomeration process also modifies the bioavailability of NPs, altering the interaction pathways with the respiratory tract to ingestion in fish [59]. Besides, the hydrodynamic diameter, zeta potential and PdI presented higher values in RW than UW, even in different pH, showing a smaller hydrodynamic diameter and more stability at pH 7 (Fig. S3).

Interaction of NPs with the embryo chorion and larval surface

SEM followed by EDS analysis showed the presence of Fe and Mn adhered at specific sites of the embryo chorion after 48 hpe of $MnFe_2O_4$ NPs (10 mg L^{-1}) from both synthesis (Fig. 2). Both NPs also induced an obstruction of chorion pore canals of zebrafish embryos (Fig. 2B,C). Previous studies have previously reported the interaction and adhesion of NMs with zebrafish chorion mediated by glycoproteins and carbohydrates on the chorion surface, which was observed not only to citrate-functionalized maghemite (γ-Fe_2O_3 NPs) [29], but also to SiO_2 NPs [60], polystyrene nanoplastics [55], and plastic microfibres from facial masks [52].

In contrast to zebrafish embryos, the larvae exposed to both $MnFe_2O_4$ NPs (10 mg L^{-1}) did not show detectable Fe or Mn in its surface body, including eye (point 1), heart (point 2), abdomen (point 3) or tail (point 4) (Fig. 3). The absence of adhesion of $MnFe_2O_4$ NPs in the larvae's body surface is probably due to the swimming behavior of the zebrafish larvae after 144 hpe, which avoid the direct accumulation in their surface. However, due to hatching, direct contact with the aquatic environment, and search for exogenous food, other interaction routes of NPs and fish larvae may occur, such as uptake by gills and ingestion, like γ-Fe_2O_3 NPs and Fe ions observed in the intestinal tract of zebrafish larvae after 144 h [29]. Thus, the NM interaction and possible accumulation in zebrafish larvae depend on their morphology and concentrations [52]. The presence of Fe and Mn in zebrafish chorion after 48 hpe and the absence of these materials in the larvae's body surface after 144 hpe may be associated with hazardous effects observed only in zebrafish embryos exposed to $MnFe_2O_4$ HT and CP NPs.

Zebrafish embryo-larval toxicity test

Survival rate

The citrate-coated $MnFe_2O_4$ NPs from both methods of synthesis did not induce changes in survival rates of zebrafish embryos and larvae in comparison with the negative control (NC) group during the exposure period ($p > 0.05$; Fig. 4A-D). This result is in accord with previous studies, in which the exposure of PEGylated MnFe-based NPs for 144 h did not induce mortality in embryo-larval zebrafish at 10 mg L^{-1}, but induced a high mortality (> 50%) at 100 mg L^{-1} [20]. Zebrafish larvae (96 h) exposed to Mn_2O_3-CMC-LA HNMs (1 mg mL^{-1}; 50–100 nm) had 100% of survival [34]. Uncoated Fe_2O_3 NPs (26 nm) from *Aerva*

Table 1 Hydrodynamic diameter (nm), Polydispersity index, and Zeta potential (mV) of manganese ferrite nanoparticles ($MnFe_2O_4$ NPs) obtained by hydrothermal and coprecipitation synthesis methods, in ultrapure water (UW) and in reconstituted water (RW). The values represent the means of analyses performed in triplicate ± standard deviation

	Hydrothermal NPs		Coprecipitation NPs	
	UW	RW	UW	RW
Hydrodynamic diameter (nm)	31.72 ± 3.31	121.05 ± 35.69	29.82 ± 1.10	334.07 ± 24.48
Zeta potential (mV)	−27.66 ± 0.36	−14.74 ± 2.10	−28.85 ± 0.55	−15.88 ± 0.37
Polydispersity index	0.37 ± 0.23	1.90 ± 0.10	0.38 ± 0.14	1.39 ± 0.73

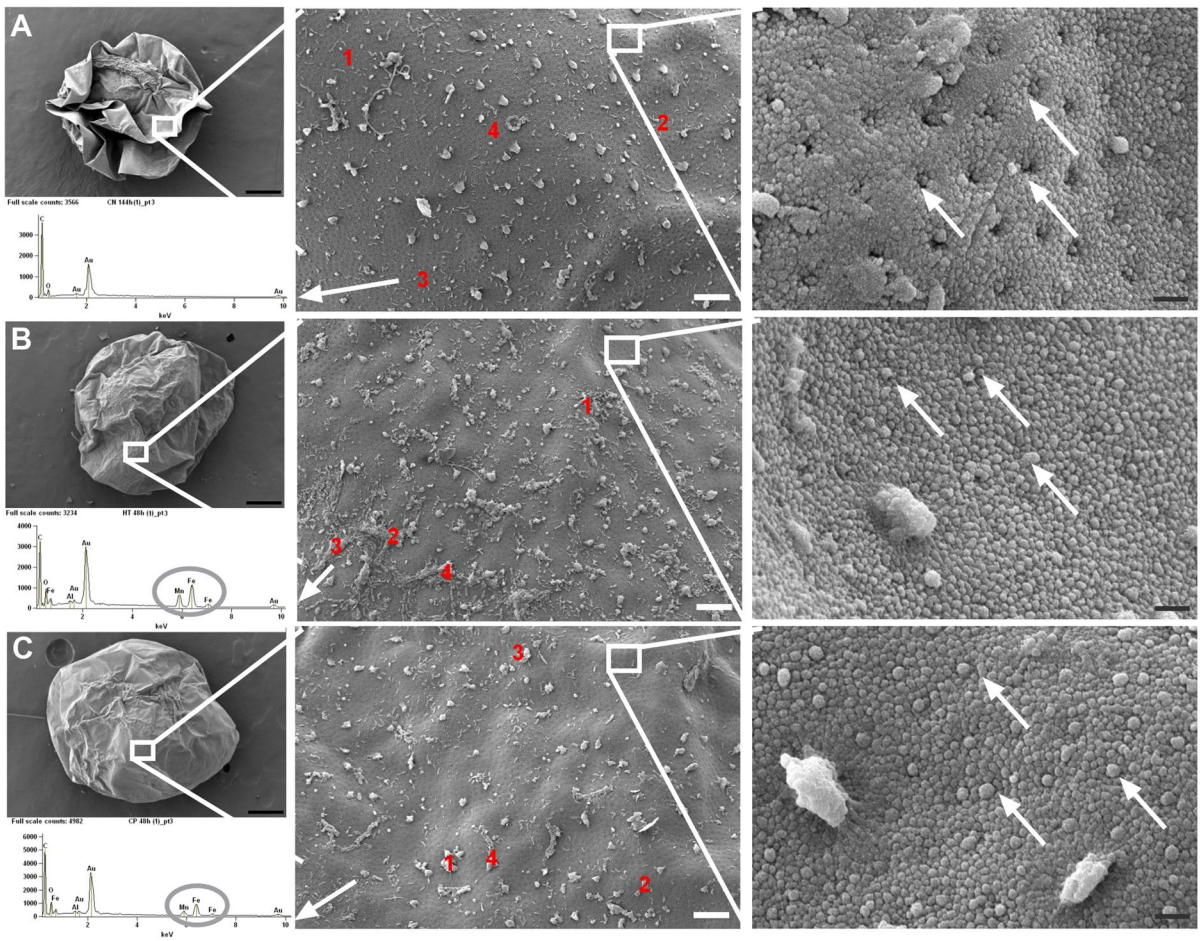

Fig. 2 Scanning electron micrographs (SEMs) and energy dispersive X-ray spectroscopy (EDS) of zebrafish embryos from negative control group **A** and after 48 h of exposure to citrate-coated $MnFe_2O_4$ NPs from Hydrothermal synthesis (HT NPs at 10 mg L^{-1}) **B** and Coprecipitation synthesis (CP NPs at 10 mg L^{-1}) **C**. The graph spectrum represents the EDS analyses, showing the presence of Fe and Mn in HT and CP NPs exposures. The arrows in the third column indicate the chorion pore canals of zebrafish embryos. The black scale bar in embryos micrographs is 200 µm; the white scale bar is 10 µm and the grey scale bar is 1 µm

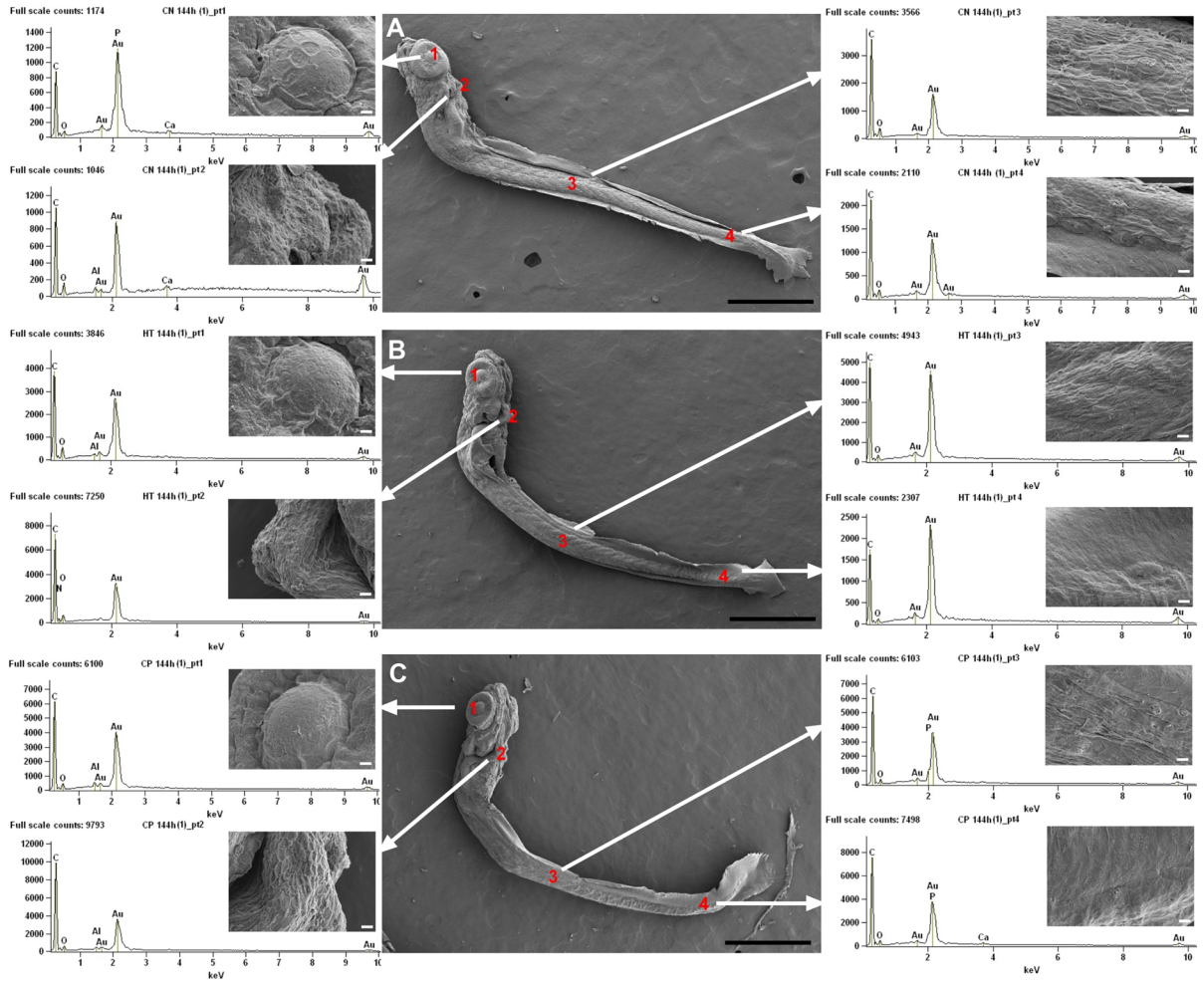

Fig. 3 Scanning electron micrographs (SEM) and energy dispersive X-ray spectroscopy (EDS) of zebrafish larvae at 144 h of exposure to citrate-coated $MnFe_2O_4$ NPs from Hydrothermal synthesis (HT NPs) and Coprecipitation synthesis (CP NPs). Negative control group **A**, 10 mg L^{-1} HT NPs **B** and CP NPs **C**. Four points of EDS analyses: eye (point 1), heart (point 2), abdomen (point 3), tail (point 4) of zebrafish larvae. The black scale bar in larvae micrographs is 500 µm and the white scale bar is 10 µm

lanata leaf extract only induced mortality at 100 and 125 mg L^{-1} [61]. Besides, the exposure of citrate-coated maghemite γ-Fe_2O_3 NPs (0.3 to 10 mg L^{-1}) during 144 h [29], and PEGylated Fe_3O_4 NPs (0.125 to 8.0 mM) for 120 h also did not induce mortality in zebrafish larvae [30], confirming that the mortality effects of IONPs on fish are concentration-dependent.

Hatching rate

Similar to the survival rate, the exposure of zebrafish embryos to HT NPs (Fig. 4E) and CP NPs (Fig. 4F) did not alter the hatching rate ($p > 0.05$). The embryos showed 100% of hatching rate until 72 h as expected, while PC had 30% of hatching rate ($p > 0.05$). Similarly, zebrafish embryos exposed to alginate hydrogels MnFe nanodots also did not alter the hatching rate [62]. Also, Mn-doped mesoporous hydroxyapatite (MnHAp) nanorods (25 mg L^{-1}) did not alter zebrafish hatching rates [63]. The exposure of citrate-coated maghemite γ-Fe_2O_3 NPs (0.3 to 10 mg L^{-1}) during 144 h also did not alter the hatching rate [29], but chitosan-coated SPIONs (8 mM) died before hatching [30], demonstrating that the coating probably influences the toxic effects.

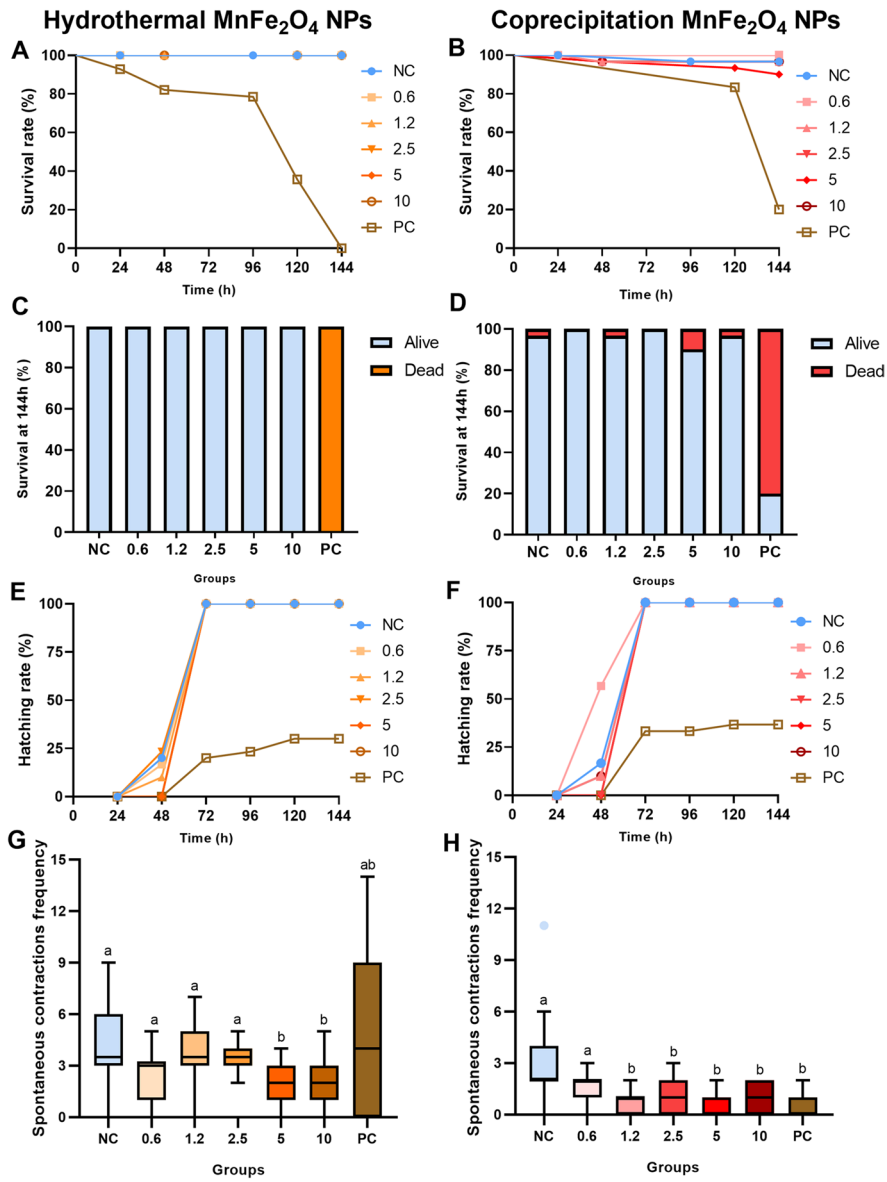

Fig. 4 Survival rate (%), hatching rate (%), and spontaneous contraction frequency—SCF (movements/min) in zebrafish from negative (NC) and positive (PC) control groups and after exposure to citrate-coated manganese ferrite nanoparticles ($MnFe_2O_4$ NPs). Survival rate of zebrafish embryos and larvae during 144 h of exposure to $MnFe_2O_4$ NPs from Hydrothermal synthesis (HT NPs) **A** and Coprecipitation synthesis (CP NPs) **B**, according to Log-Rank test. Survival at 144 h of exposure to HT NPs **C** and CP NPs **D**, according to Log-Rank test. Hatching rate of zebrafish during 144 h of exposure to HT NPs **E** and CP NPs **F**, according to Log-Rank test. SCF of zebrafish embryos at 24 h post exposure to HT NPs **G** and CP NPs **H**, according to Kruskal–Wallis test and post hoc Dunn's test. Zebrafish were exposed to several concentrations of both NPs (0.6, 1.25, 2.5, 5, and 10 mg $L.^{-1}$). Distinct letters indicate significantly different results between experimental groups ($p < 0.05$), while the same letters indicate non-significantly different results ($p > 0.05$)

Neurodevelopmental effects

After 24 hpe, both NPs reduced the SCF in zebrafish embryos in comparison with those unexposed ($p < 0.05$; Fig. 4G,H). The exposure of embryos to the two higher concentrations of HT NPs (5 and 10 mg L^{-1}) reduced the SCF, when compared to the NC group ($p < 0.01$ and $p < 0.01$; respectively) (Fig. 4G). Similar results happened with the following concentrations of CP NPs: 1.25 mg L^{-1} ($p < 0.01$), 2.5 mg L^{-1} ($p < 0.01$), 5 mg L^{-1} ($p < 0.01$), and 10 mg L^{-1} ($p < 0.01$) (Fig. 4H). SCF is commonly used as an indicator of neurodevelopmental effects, and the mechanism reported for IONPs include neurotoxicity can involve alterations in genetic expression and changes in the development of neurons and muscles [64]. For example, extremely small IONPs (ESIONPs) (~3 nm; 40 mg L^{-1}) downregulated the expression of neuronal developmental (*pax2a*, *neurog1*, *axin2*) and muscle markers (*acta2*, *ttn*, *lpin1*) in zebrafish larvae after exposure to 72 hpf [64]. Then, ESIONPs altered neuronal development,

consequently the synaptic signal transmission, neuromuscular junction signal transmission, and reduced muscle development [64].

The SCF alterations were detected even in lower concentrations of CP NPs when compared to HT NPs. A possible explanation is related to iron release from CP NPs, according to the higher presence of iron on the surface of these NPs arising from the passivation process in their synthesis, considering the methodology steps [65], although this remains to be verified. Besides, another factor that could have influenced this effect is the instability of CP NPs in RW, as seen in Table 1.

The nanobiointeraction of IONPs and the presence of iron ions in zebrafish chorions were already reported by SEM and EDS analysis after 48 h of citrate-functionalized γ-Fe_2O_3 NPs exposure [29]. In addition to the adhesion process, the $MnFe_2O_4$ NPs may interact with or penetrate the chorion, since their size is smaller than the zebrafish pore size, which can reach 500—700 nm [66]. Agglomerates/aggregates of NPs can block the pores, disturbing the gas and metabolite exchange, potentially leading to hypoxic conditions [67]. This argument corroborates the obstruction of chorion pore canals shown in SEM results (Fig. 2). Hypoxia is usually related to neurotoxicity, because the lack of oxygen conditions can reduce the number of diencephalic dopaminergic (DA) neurons at 48 hpf zebrafish [68].

Cardiotoxicity

The exposure of zebrafish embryos to both $MnFe_2O_4$ NPs induced differential heartbeat rate in comparison with the NC group ($p < 0.05$; Fig. 5A-D). HT NPs induced tachycardia in zebrafish embryos of 48 hpe for the concentrations of 5 mg L^{-1} ($p < 0.05$) and 10 mg L^{-1} ($p < 0.01$) (Fig. 5A), while CP NPs induced bradycardia in zebrafish embryos of 48 hpe for the concentrations of 2.5 mg L^{-1} ($p < 0.01$), 5 mg L^{-1} ($p < 0.01$) and 10 mg L^{-1} ($p = 0.05$) (Fig. 5B). Almost all PC individuals presented bradycardia, as previously reported [55]. The decrease in heartbeat rate in zebrafish embryos exposed to uncoated Fe_2O_3 (40 ppm) was related to oxidative stress [31], due to the excessive ROS production by the Fenton reaction [69]. Besides, ultrasmall (USPIONs) Fe_3O_4 NPs (2.3 and 4.2 nm) at 100 mg kg^{-1} induced acute cardiac failure and death of mice [70], demonstrating that cardiotoxic effects induced by IONPs have been reported. USPIONs toxicity was associated with the highest ROS level, to the iron element and size [70]. The toxicity of metal oxide NPs may depend on the NPs themselves, or on the release of ions from the NPs, or induced by both forms [71].

Although Wang et al. (2016) [71] did not detect iron ions after 96 h of the stock Fe_2O_3 NPs dispersion preparation, previous studies with zebrafish already associated the iron release with the toxic effects of IONPs [64, 72]. The IONPs may release iron ions and also lead to iron accumulation, resulting in DNA damage, cytotoxicity, inflammatory processes, and homeostasis dysregulation [72]. Besides, the exposure of iron ions in concentrations similar (0.3—10 mg L^{-1}) to the ones used in the present study, induced more toxic effects than the exposure of IONPs [29]. Thus, an example of mechanism of action is that some of the $MnFe_2O_4$ NPs could have entered the chorion, which could lead to oxidative stress in cardiac tissue. While NPs agglomerates probably blocked the chorion pores, leading to hypoxia [67], affecting embryonic homeostasis. It is important to emphasize that the neurotoxic and cardiotoxic effects were both quantified in the period that the most animals are still inside the chorion. After hatching (72 hpf), the zebrafish larvae presented normal aspects, which may be associated with pos-hatching physiological recovery.

Although the described cardiotoxic effects, the percentages of individuals with bradycardia and tachycardia were lower than 50% (Fig. 5C,D). The group of 5 mg L^{-1} HT NPs showed 63.33% of zebrafish embryos with normal heartbeat and 36.67% had tachycardia ($p < 0.01$), while for 10 mg L^{-1} HT NPs group, 80% of zebrafish embryos had normal heartbeat and only 20% had tachycardia ($p > 0.05$) (Fig. 5C). On the other hand, the percentage of zebrafish embryos with bradycardia was lower than 35% for CP NPs exposed groups (Fig. 5D), except by the 2.5 mg L^{-1} group, which showed 40% of zebrafish embryos with bradycardia and 60% with normal heartbeat ($p < 0.05$). Green citrate-coated Fe_3O_4 NPs synthesized from the extract of *P. niruri* also induced bradycardia in zebrafish embryos, but only above the concentration of 10 mg L^{-1} [32]. However, static exposure of citrate-coated γ-Fe_2O_3 NPs (size = 3.97 ± 0.85 nm) until 10 mg L^{-1} did not induce bradycardia nor tachycardia in 48 h zebrafish

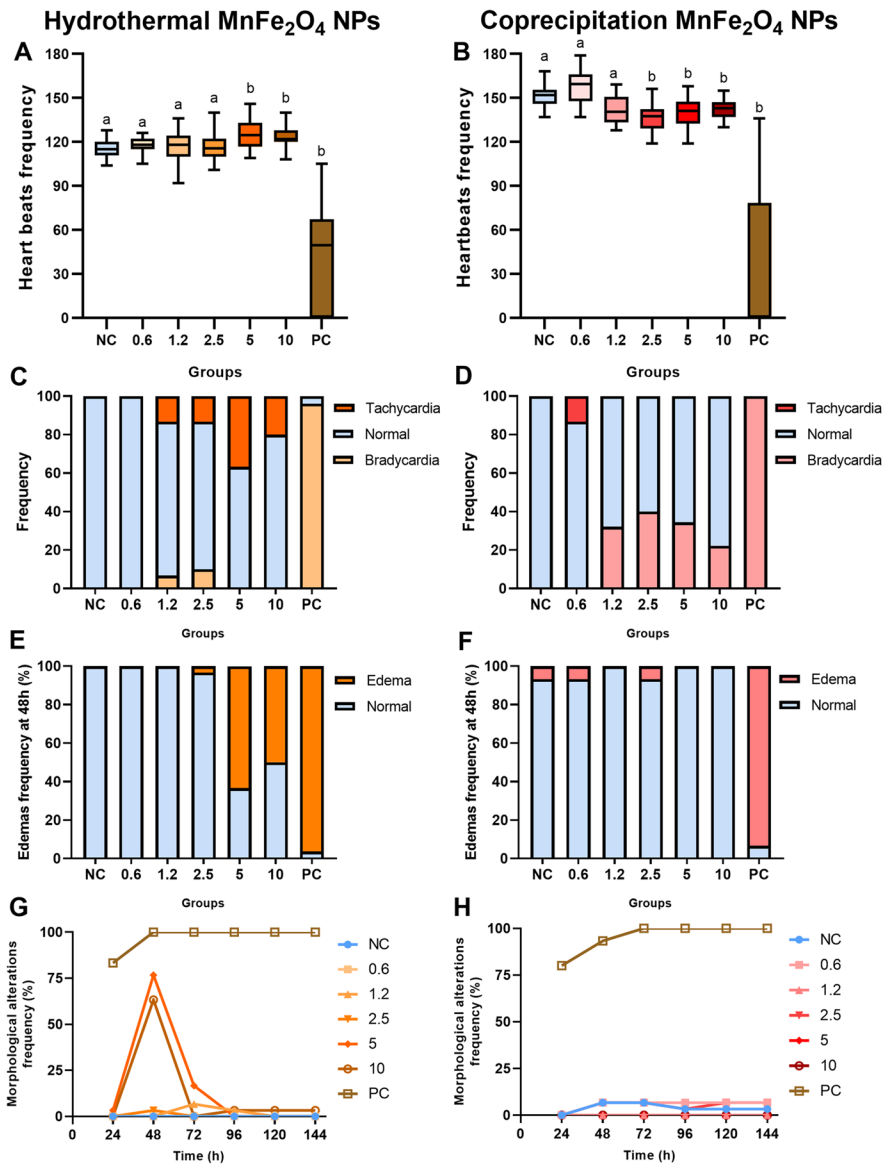

Fig. 5 Heartbeat rate (beats/minute) and morphological alterations frequency (%) in zebrafish from negative (NC) and positive (PC) control groups and after exposure to citrate-coated manganese ferrite nanoparticles ($MnFe_2O_4$ NPs). Heartbeat rate (beats/minute) of zebrafish embryos at 48 h post exposure to $MnFe_2O_4$ NPs from Hydrothermal synthesis (HT NPs) **A** and Coprecipitation synthesis (CP NPs) **B**, according to Kruskal–Wallis test and post hoc Dunn's test. Frequency of tachycardia and bradycardia in zebrafish embryos at 48 h post exposure to HT NPs **C** and CP NPs **D**, according to Kruskal–Wallis test and post hoc Dunn's test. Frequency of edemas in zebrafish embryos at 48 h post exposure to HT NPs **E** and CP NPs **F**, according to Kruskal–Wallis test and post hoc Dunn's test. Morphological alterations frequency of zebrafish embryos and larvae during 144 h of exposure to HT NPs **G** and CP NPs **H**, according to Kruskal–Wallis test and post hoc Dunn's test. Zebrafish were exposed to several concentrations of both NPs (0.6, 1.25, 2.5, 5, and 10 mg $L.^{-1}$). Distinct letters indicate significantly different results between experimental groups ($p < 0.05$), while the same letters indicate non-significantly different results ($p > 0.05$)

embryos [29], so the presence of Mn can result in different effects of other iron NPs.

Another cardiotoxic-related effect detected was the pericardial edemas in 48 hpe zebrafish embryos, as can be seen in concentrations of 5 mg L^{-1} ($p < 0.01$) and 10 mg L^{-1} ($p < 0.01$) of HT NPs (Fig. 5E,F). CP NPs groups did not induce significant edemas ($p > 0.05$) (Fig. 5E,F). However, the pericardial edemas were reabsorbed in the following days of exposure (Fig. 5G,H), with no apparent sequelae, so this was a transient effect. Pericardial edema was also observed in higher concentrations of Fe_3O_4 NPs, such as 20 mg L^{-1} exposure in zebrafish embryos [32]. Edemas are caused by osmotic imbalance and are directly related to the lymphatic system, due to the accumulation of interstitial fluid, increasing the tissue volume [73]. The reabsorption process involves lymphangiogenesis, which is essential in restoring normal fluid balance through the expansion of lymphatic vessels to fluid drainage [73].

Morphological alterations

HT NPs and CP NPs exposure did not induce significant morphological alterations in zebrafish larvae after 72 hpe (Fig. 5G,H; Table S1; Table S2). MnHAp nanorods (25 mg L^{-1}) did not induce zebrafish morphological alterations up to 96 h [63]. Mn_2O_3-CMC-LA HNMs (1 mg mL^{-1}) had also no morphological deformities detected in zebrafish up to 96 h [34]. ESIONPs induced malformations in zebrafish only in the exposed groups above 10 mg L^{-1}, which were: dorsal bending, shortened body length, yolk sac swelling, cardiac edema, smaller eyes and head [64]. Fe_2O_3 NPs (26 nm) synthesized from the *A. lanata* leaf extract were biocompatible up to 50 mg L^{-1} to zebrafish after 48, 72, and 96 hpf, but 75, 100 and 125 mg L^{-1} presented malformations [61]. Besides, uncoated Fe_3O_4 NPs induced microcephaly and yolk malabsorption in zebrafish at 36 hpe above 50 mg L^{-1} [74], demonstrating that the NPs concentration is a relevant factor involved in zebrafish morphological alterations. However, edemas in the PC groups were much more noticeable than the $MnFe_2O_4$ NPs exposure groups (Fig. 6). Furthermore, the $MnFe_2O_4$ NPs, mainly from CP synthesis, had adhesion to the surface of zebrafish chorions, also altering their color (Fig. 6), in accordance with the SEM results (Fig. 2).

Considering translational research, IONPs effects described in mammals can also support the insights of mechanism of action of these NPs on zebrafish models. Cardiotoxic effects of IONPs were already described in mice, causing a reduction in blood pressure and cardiac dysfunction [75] and in male rats by long-term exposure to IONPs [17]. On the other hand, MnFe-based NPs induced alterations of blood pressure in isolated perfused rat hearts (ex vivo), but not in conscious rats (in vivo) [76]. Furthermore, albumin coating can reduce cardiac effects of magnetic NPs, due to the interaction between NPs with biomolecules in the biological fluids, forming the corona protein, which can prevent the NP internalization in the cardiac cells [77]. Another strategy is the addition of an iron chelator, like deferoxamine, which reduced the ROS generation by IONPs and also, deferoxamine PEG/Dextran-coated SPIONs (synthesized via the coprecipitation method) applied to mice (2 mg mL^{-1}) reduced the liver bioaccumulation [78]. Finally, the absence of Fe and Mn in the larvae's body surface after 144 hpe (Fig. 3) is in accordance with the no hazardous effects after hatching.

Reactive oxygen species

After 144 h of exposure, the $MnFe_2O_4$ NPs of both syntheses did not alter the ROS levels in zebrafish larvae ($p > 0.05$; Fig. 7A,B), and did not alter the protein quantified by Bradford (Fig. S4). On the other hand, green citrate-coated Fe_3O_4 NPs synthetized from the extract of *P. niruri* induced ROS in zebrafish larvae after exposed NPs from 5 to 250 mg L^{-1}, detected by flow cytometer [32]. Zebrafish embryos exposed to uncoated Fe_3O_4 NPs (50 mg L^{-1}) increased lipid peroxidation—LPO (elevated malondialdehyde levels), reduced antioxidant capacity (decreased glutathione content and superoxide dismutase—SOD activity) [74], detecting specific molecules instead of ROS in general. These Fe_3O_4 NPs at 100 mg L^{-1} also downregulated two major regulators of the ferroptosis pathway (GPX4 and xCT) [74]. IONPs are capable of inducing redox imbalance and dysregulation of ferroptosis-related genes [74], depending on the concentration. However, green uncoated Fe_2O_3 NPs (26 nm) from *A. lanata* leaf extract curiously showed the ability to reduce oxidative stress induced by hydrogen peroxide

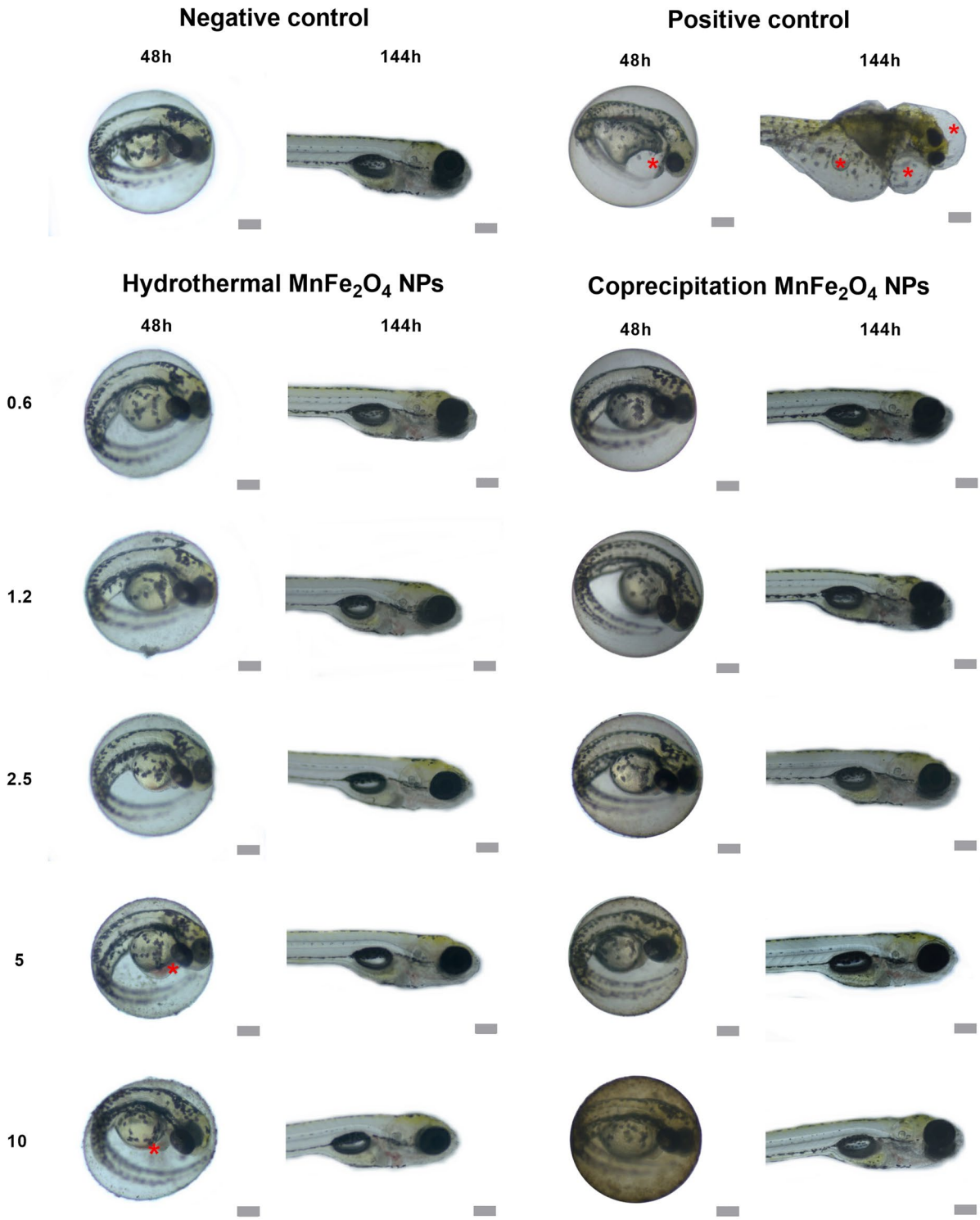
Negative control
48h
144h
Positive control
48h
144h
Hydrothermal $MnFe_2O_4$ NPs
48h
144h
Coprecipitation $MnFe_2O_4$ NPs
48h
144h
0.6
1.2
2.5
5
10

◂**Fig. 6** Photomicrographs of zebrafish embryos (48 h) and larvae (144 h) from negative (NC) and positive (PC) control groups and after exposure to citrate-coated manganese ferrite nanoparticles ($MnFe_2O_4$ NPs) from Hydrothermal synthesis (HT NPs) and Coprecipitation synthesis (CP NPs). Zebrafish were exposed to several concentrations of both NPs (0.6, 1.25, 2.5, 5, and 10 mg L^{-1}). The scale bar is 200 µm. The asterisk indicates morphological alterations, such as pericardial edema, yolk sac edema, alteration in curvature and head malformation

in zebrafish embryos [61]. The embryos were pre-treated with the Fe_2O_3 NPs (10 to 40 mg L^{-1}) and then exposed to H_2O_2 (5 mM), provoking the reduction of ROS and MDA levels, and increasing activity of antioxidant enzymes (GSH, CAT, and SOD) [61].

In the same way, a hybrid nanomaterial with Mn (mPDA-SeMn-IR) composed of enzyme-like 2-(phenylselanyl)ethan-1-amine (SePh) and manganese dioxide (MnO_2) and NIR-II absorber IR-1048 (IR) integrated onto the mesoporous polydopamine (mPDA) core, was capable of eliminating excessive ROS in a zebrafish larvae Parkinson disease model [79]. This is due to the importance of Mn in antioxidant factors, also exercising a cofactor role in Mn-dependent SOD, mainly localized in the inner membranes of mitochondria [80]. In a study with rats and SH-SY5Y cells, the exposure of Mn, Fe, and Mn-Fe induced oxidative stress, increasing the expression of *Bcl2, Bax, α-syn* and activating the inflammatory factors IL-6 and IL-12, but the combined Mn-Fe exposure attenuated the oxidative stress when compared to the isolated Mn and Fe exposures [81]. The combined Mn-Fe increased the expression of antioxidant factors Nrf2, HO-1, and NQO1 (stress-related proteins) [81]. However, PC-12 rat cells exposed to Mn NPs (40 nm) had a tenfold increase in ROS levels higher than the control group, inducing oxidative stress [82]. Based on this, the results in the present study showed no ROS imbalance after 144 h of exposure, but we can not infer if this is related to the presence of Mn in the NPs or to exposure conditions.

Cell viability

HT and CP $MnFe_2O_4$ NPs did not affect the cell viability of zebrafish larvae after 144 hpe ($p > 0.05$; Fig. 7C-H; Fig. 8). Although there are already reports of metallic oxide NPs altering cell viability in zebrafish larvae [31, 32], the concentrations used were higher than those utilized in the present study. Green citrate-coated Fe_3O_4 NPs synthetized from the extract of *P. niruri* at 20 to 250 mg L^{-1} induced apoptosis in zebrafish larvae after 72 hpe [32]. Besides, uncoated Fe_2O_3 NPs (40 and 60 mg L^{-1}) provoked a high incidence of apoptotic bodies in zebrafish larvae when compared to the control [31]. It is known that cell death induced by IONPs is related to ferroptosis, and the cascade reaction is conserved in vertebrate embryos, such as chicken and zebrafish embryos [74], but it depends on the concentration and specific characteristics of the IONPs.

Behavioral analysis

The exposure to HT NPs and CP NPs (Fig. 9) did not alter the behavior of zebrafish larvae at 144 h ($p > 0.05$). All the parameters analyzed of zebrafish larvae exposed to both NPs (mean speed (cm/s), maximum speed (cm/s), total distance traveled (cm), time in peripheric area (s), time in central area (s), total latency time (s) did not have significant difference in comparison with negative control group ($p > 0.05$; Fig. 9). However, chitosan-coated Fe_3O_4 NPs (0.125 mM) induced decrease in the distance traveled by zebrafish larvae at 120 h post-fertilization when compared to the control [30]. On the other hand, the zebrafish larvae of 144 h in the present study did not demonstrate locomotor behavioral effects.

Principal Component Analysis (PCA)

PCA was used to explore multivariate patterns across experimental groups. Results confirmed the similarity in response between the zebrafish embryos and larvae in the negative control group and those in the groups exposed to both NPs (Fig. 10). The first two components explained 55.6% of the total variance (PC1 = 42.1%; PC2 = 13.5%). PC1 was primarily associated with physiological and behavioral endpoints, including ROS levels, cell viability, heartbeats (cardiac function), locomotor activity, and spatial distribution parameters. PC2 was mainly driven by variability in cell viability and locomotor parameters. Thus, the clustering pattern indicated substantial overlap between control and NP-exposed groups, suggesting that, at the tested concentrations, most endpoints

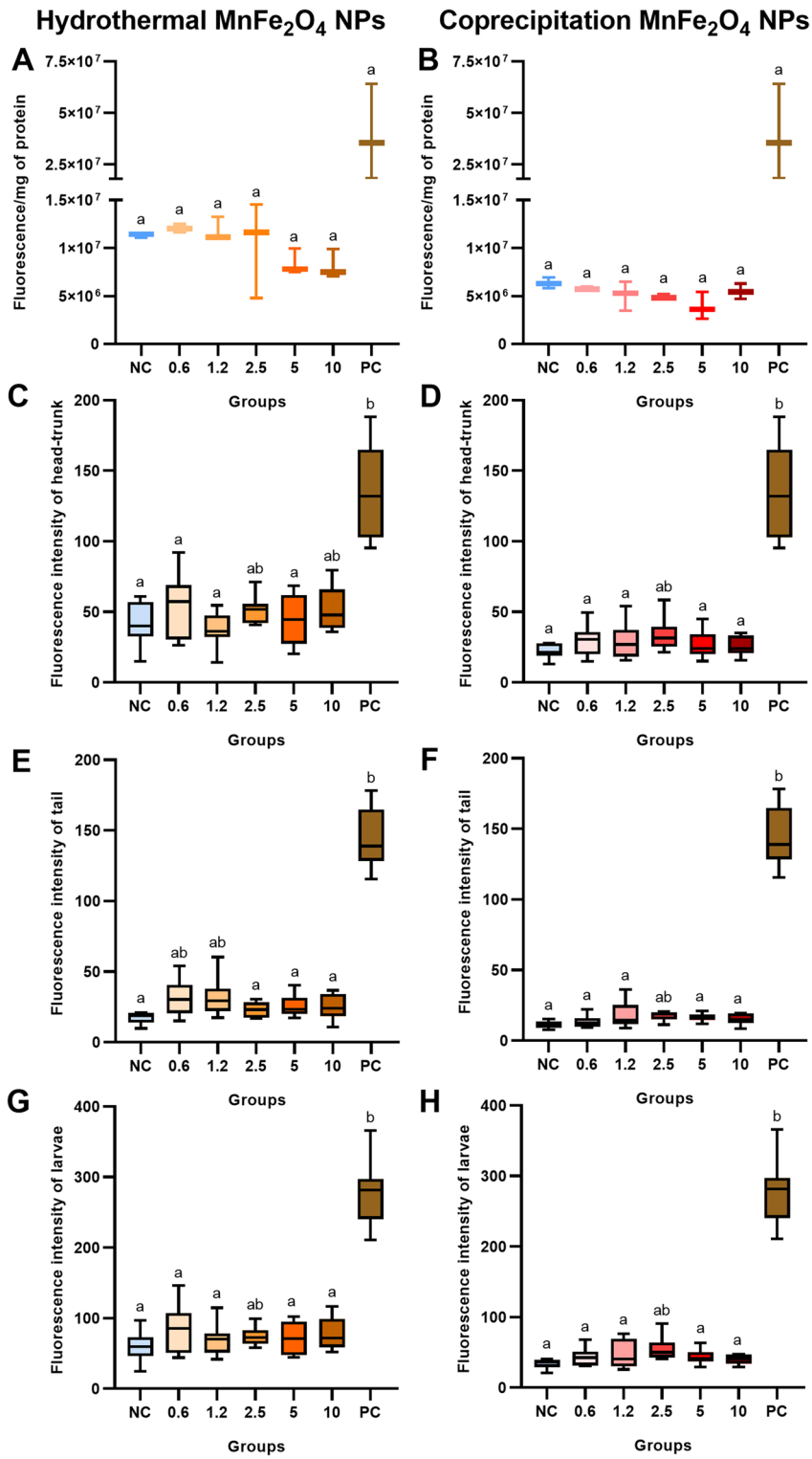

Fig. 7 Reactive oxygen species (ROS) levels in zebrafish larvae from negative (NC) and positive (PC) control groups and after exposure to citrate-coated manganese ferrite nanoparticles ($MnFe_2O_4$ NPs). ROS levels in zebrafish larvae after 144 h of exposure to $MnFe_2O_4$ NPs from Hydrothermal synthesis (HT NPs) **A** and Coprecipitation synthesis (CP NPs) **B**, according to Kruskal–Wallis test and post hoc Dunn's test. Cell viability according to Kruskal–Wallis test and post hoc Dunn's test, of zebrafish head and trunk HT NPs **C** and CP NPs **D**. Cell viability of zebrafish tail HT NPs **E** and CP NPs **F**. Cell viability of zebrafish larvae HT NPs **G** and CP NPs **H**. Zebrafish were exposed to several concentrations of both NPs (0.6, 1.25, 2.5, 5, and 10 mg $L.^{-1}$). Distinct letters indicate significantly different results between experimental groups ($p < 0.05$), while the same letters indicate non-significantly different results ($p > 0.05$)

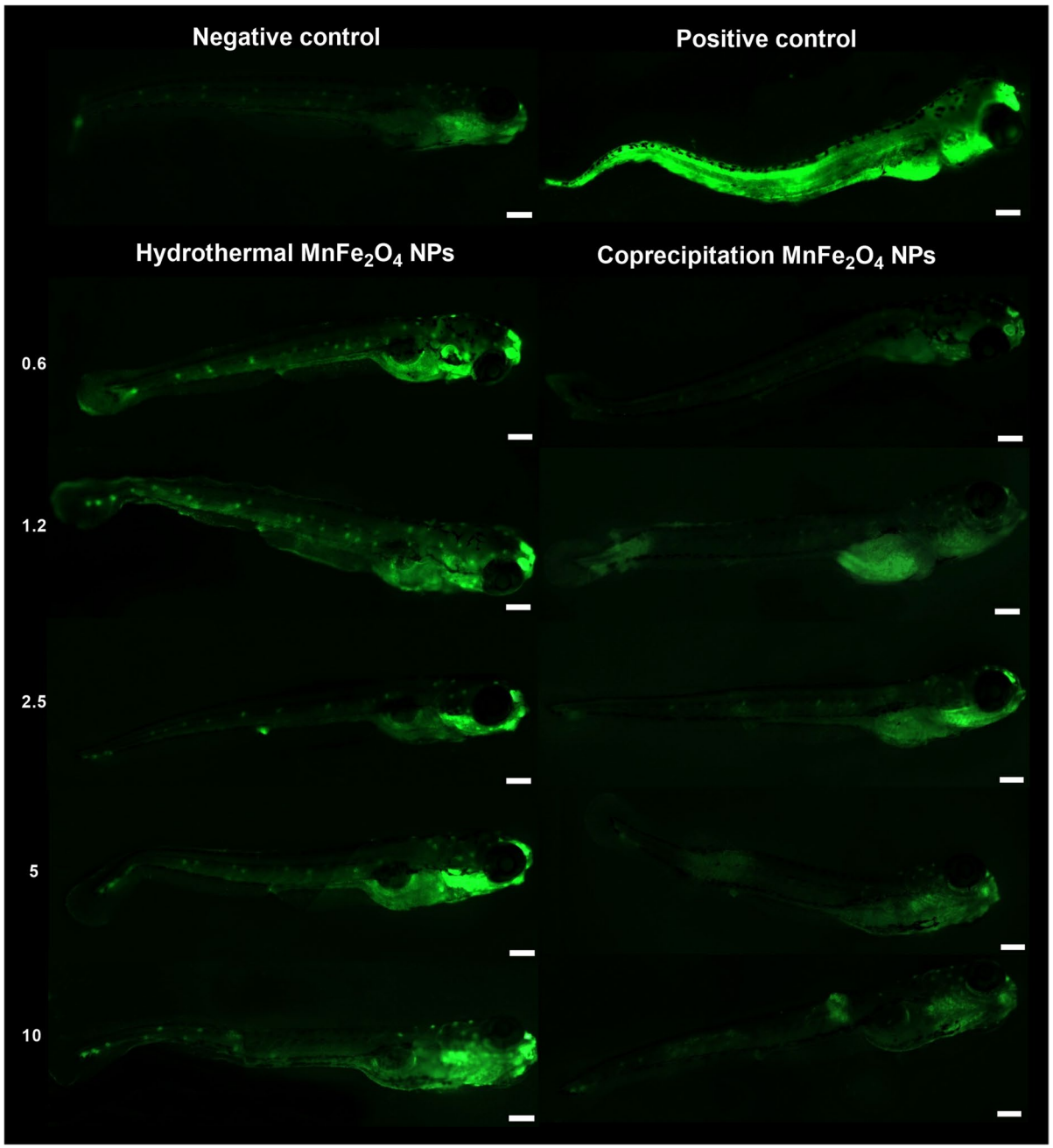

Fig. 8 Fluorescence photomicrographs of cell viability of zebrafish larvae from negative (NC) and positive (PC) control groups and after 144 h of exposure to citrate-coated manganese ferrite nanoparticles ($MnFe_2O_4$ NPs) from Hydrothermal synthesis (HT NPs) and Coprecipitation synthesis (CP NPs). Zebrafish were exposed to several concentrations of both NPs (0.6, 1.25, 2.5, 5, and 10 mg L^{-1}). The scale bar is 200 µm

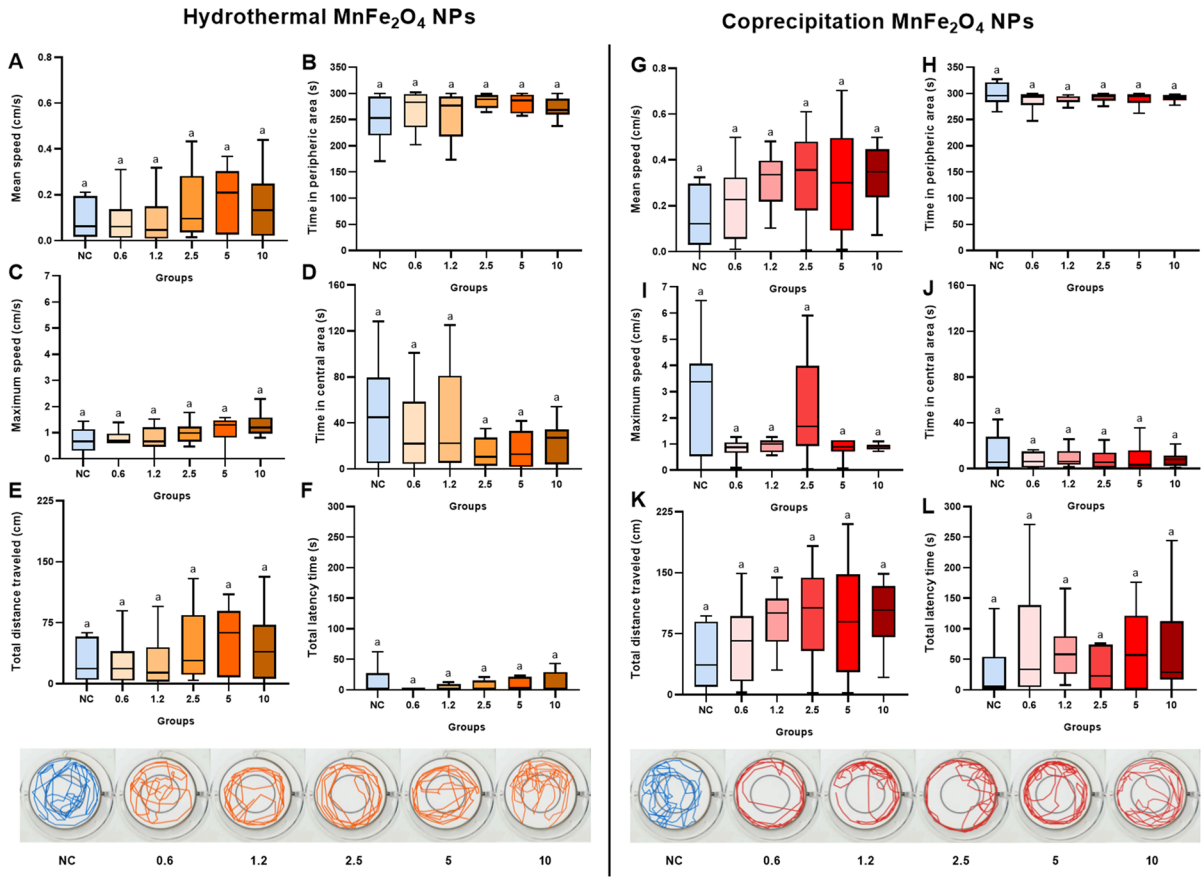

Fig. 9 Behavioral parameters in zebrafish larvae from negative (NC) and positive (PC) control groups and after exposure to citrate-coated manganese ferrite nanoparticles ($MnFe_2O_4$ NPs) from Hydrothermal synthesis (HT NPs) and Coprecipitation synthesis (CP NPs), according to Kruskal–Wallis test and post hoc Dunn's test. Mean speed (cm/s) HT NPs **A** and CP NPs **G**, time in peripheric area (s) HT NPs **B** and CP NPs **H**, maximum speed (cm/s) HT NPs **C** and CP NPs **I**, time in central area (s) HT NPs **D** and CP NPs **J**, total distance traveled (cm) HT NPs **E** and CP NPs **K**, total latency time (s) HT NPs **F** and CP NPs **L**. Representative larvae path of HT NPs and CP NPs. Zebrafish were exposed to several concentrations of both NPs (0.6, 1.25, 2.5, 5, and 10 mg $L.^{-1}$). Distinct letters indicate significantly different results between experimental groups ($p < 0.05$), while the same letters indicate non-significantly different results ($p > 0.05$)

were not differentiated by exposure condition. This multivariate pattern supports the absence of consistent post-hatching effects and indicates that early sublethal responses did not translate into broader systemic alterations at later developmental stages.

The current study confirms that the analysis of multiple biomarkers in zebrafish embryos and larvae is an important approach to better understanding the effects of NMs on aquatic organisms. This approach was previously reported for plastic microfibres from facial masks [52] and polystyrene nanoplastics [55] in zebrafish, and green silver NPs from *Croton urucurana* on *Biomphalaria glabrata* [83]. Overall, the PCA showed similar responses observed between zebrafish embryos and larvae from control, HT and CP NPs groups at the concentrations analysed.

Conclusion

$MnFe_2O_4$ NPs of different synthesis induced different early developmental effects on zebrafish. The synthesis method, jointly with NP size and surface, may influence their effects in zebrafish. Fe and Mn were detected in zebrafish chorion exposed to the higher concentration of HT and CP NPs, but they were not

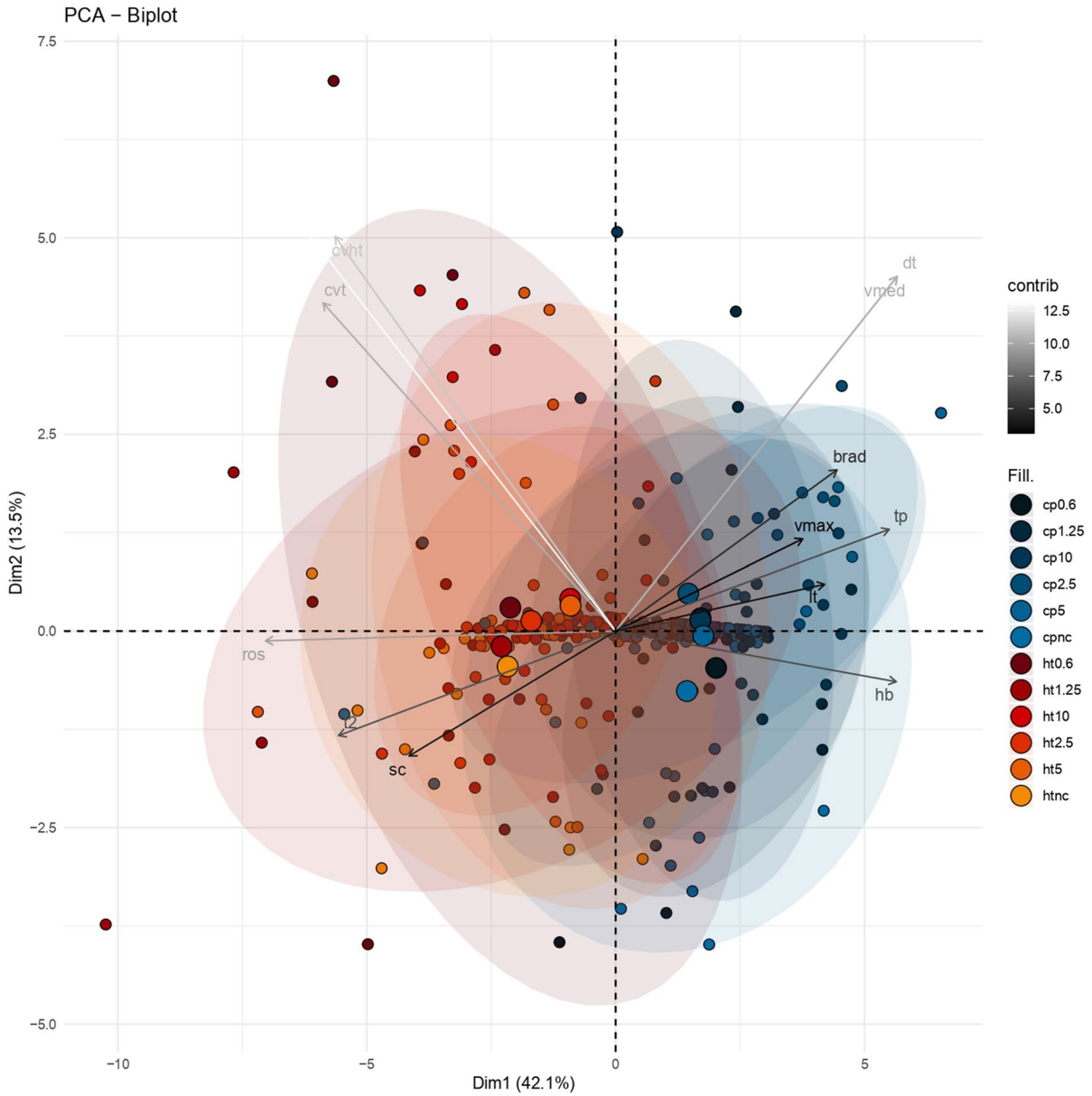

Fig. 10 Principal component analysis (PCA) of multiple biomarkers responses in zebrafish embryos and larvae from negative (NC) control groups and after exposure to citrate-coated manganese ferrite nanoparticles ($MnFe_2O_4$ NPs) from Hydrothermal synthesis (HT NPs) and Coprecipitation synthesis (CP NPs). Spontaneous contractions (sc), heartbeats (hb), medium velocity (vmed), maximum velocity (vmax), total distance (dt), peripheral time (tp), time in area 2 (t2), total latency (lt), ROS (ros), cell viability of head and trunk (cvht), cell viability of tail (cvt), cell viability of larvae (cvl) and protein quantification by bradford (brad)

present on the larvae's body surface, indicating interaction with the zebrafish chorion. HT and CP NPs did not induce mortality or hatching inhibition. Sublethal effects were related to neurotoxicity and cardiotoxicity at 24 and 48 hpe. However, the following days of exposure did not significantly affect morphology, ROS levels, cell viability, or locomotor behavior. Also, the pericardial edemas identified in 48 hpe were reabsorbed. Overall, synthesis-dependent early developmental effects were observed, with no evidence

of persistent post-hatching toxicity under the experimental conditions. The current study supports the use of zebrafish as a suitable model of the NPs' toxicity, comparing different synthesis methods.

Acknowledgements J. C. J. was supported by the Coordination for the Improvement of Higher Education Personnel—CAPES (proc. n. 88887.957582/2024-00). T. L. R. is granted a productivity fellowship from National Council for Scientific and Technological Development—CNPq (proc. n. 314413/2023-5). The authors acknowledge the Multi-User Centre for Animal Production and Experimentation in the Institute of Tropical Pathology and Public Health (CMPEA-IPTSP) to support the creation and maintenance of zebrafish. The authors also acknowledge the Regional Center for Technological Development and Innovation of Federal University of Goiás (CRTI-UFG) and the Multiuser High Resolution Microscopy Laboratory (LabMic-UFG) to support the characterization of NPs and Electronic Microscopy of zebrafish embryos and larvae.

Author contribution J.C.J.: conceptualization, methodology, investigation, formal analysis, data curation, writing-original draft, writing-reviewing and editing. B.L.C.: methodology, investigation, formal analysis, writing-reviewing and editing. V.G.R.S.: methodology, investigation, formal analysis, writing-reviewing and editing. M.V.A.: methodology, investigation, formal analysis, writing-reviewing and editing. A.F.B.: supervision, resources, investigation, writing-reviewing and editing. T.L.R.: conceptualization, supervision, resources, investigation, formal analysis, writing-original draft, writing-reviewing and editing.

Funding The Article Processing Charge (APC) for the publication of this research was funded by the Coordenação de Aperfeiçoamento de Pessoal de Nível Superior - Brasil (CAPES) (ROR identifier: 00x0ma614). This work was supported by a productivity fellowship from the National Council for Scientific and Technological Development—CNPq (proc. n. 314413/2023–5) and from the Coordination for the Improvement of Higher Education Personnel—CAPES (proc. n. 88887.957582/2024–00).

Data availability Data will be made available on request.

Declarations

Ethical approval Ethical and professional conduct have been followed. All animal procedures were previously approved by the Ethics Committee on Animal Experimentation of the Federal University of Goiás (CEUA—UFG), N. 73/22.

Competing interests The authors declare no competing interests.

References

1. Akhlaghi N, Najafpour-Darzi G (2021) Manganese ferrite ($MnFe_2O_4$) nanoparticles: from synthesis to application -a review. J Ind Eng Chem 103:292–304. https://doi.org/10.1016/j.jiec.2021.07.043
2. Leal MP, Rivera-Fernández S, Franco JM, Pozo D, De La Fuente JM, García-Martín ML (2015) Long-circulating PEGylated manganese ferrite nanoparticles for MRI-based molecular imaging. Nanoscale 7:2050–2059. https://doi.org/10.1039/c4nr05781c
3. Ribeiro CE, Vinícius-Araújo M, Bakuzis AF (2025) Multicore Manganese Ferrite nanoparticles for theranostics. ACS Appl Nano Mater 8:7061–7072. https://doi.org/10.1021/acsanm.5c00309
4. Cintra ER, Hayasaki TG, Sousa-Junior AA, Silva ACG, Valadares MC, Bakuzis AF et al (2022) Folate-targeted PEGylated magnetoliposomes for hyperthermia-mediated controlled release of Doxorubicin. Front Pharmacol 13:1–12. https://doi.org/10.3389/fphar.2022.854430
5. Sousa-Junior AA, Mello-Andrade F, Rocha JVR, Hayasaki TG, de Curcio JS, Silva LdoC et al (2023) Immunogenic cell death photothermally mediated by erythrocyte membrane-coated magnetofluorescent nanocarriers improves survival in sarcoma model. Pharmaceutics. https://doi.org/10.3390/pharmaceutics15030943
6. Rocha JVR, Krause RF, Ribeiro CE, Oliveira NCdeA, Ribeiro de Sousa L, Leandro Santos J et al (2025) Near infrared biomimetic hybrid magnetic nanocarrier for MRI-guided thermal therapy. ACS Appl Mater Interfaces 17:13094–13110. https://doi.org/10.1021/acsami.4c03434
7. Capistrano G, Rodrigues HF, Zufelato N, Gonçalves C, Cardoso CG, Silveira-Lacerda EP et al (2020) Noninvasive intratumoral thermal dose determination during in vivo magnetic nanoparticle hyperthermia: combining surface temperature measurements and computer simulations. Int J Hyperthermia 37:120–140. https://doi.org/10.1080/02656736.2020.1826583
8. Huang X, Wang X, Liu X, Cheng L, Pan J, Yang X (2024) Nanotechnology in agriculture: Manganese Ferrite nanoparticles as a micronutrient fertilizer for wheat. Plants. https://doi.org/10.3390/PLANTS13101395
9. Chen T, Wang X, Zhu X, Shao H, Wang W, Hua W et al (2025) Manganese Ferrite nanoparticle-assisted enhancement of photosynthetic carbon sequestration in microalgae. Sustainability 17:4303. https://doi.org/10.3390/SU17104303

10. Raie DS, Tsonas I, Mourdikoudis S, Delli E, Makridis A, Ciric L et al (2025) Protection of *Shewanella oneidensis* MR-1 by manganese ferrite nanoparticles during chromate bio-reduction. Environ Sci Nano 12:3035–3046. https://doi.org/10.1039/D5EN00204D
11. Hosseini NM, Sheshmani S, Shahvelayati AS (2024) Manganese ferrite-graphite oxide-chitosan nanocomposite for efficient dye removal from aqueous and textile wastewater under UV and sunlight irradiation. Sci Rep 15(1):1–18. https://doi.org/10.1038/s41598-024-84569-9
12. Sousa J, Pinto J, Barbosa H, Tavares DS, Freitas R, Trindade T et al (2025) Efficient recovery of gadolinium from contaminated waters using manganese ferrite nanoparticles. Recycling 10:57. https://doi.org/10.3390/RECYCLING10020057/S1
13. Soetaert F, Korangath P, Serantes D, Fiering S, Ivkov R (2020) Cancer therapy with iron oxide nanoparticles: agents of thermal and immune therapies. Adv Drug Deliv Rev 163–164:65–83. https://doi.org/10.1016/J.ADDR.2020.06.025
14. Hjorth R, Coutris C, Nguyen NHA, Sevcu A, Gallego-Urrea JA, Baun A et al (2017) Ecotoxicity testing and environmental risk assessment of iron nanomaterials for sub-surface remediation – recommendations from the FP7 project NanoRem. Chemosphere 182:525–531. https://doi.org/10.1016/J.CHEMOSPHERE.2017.05.060
15. Rio ISR, Rodrigues ARO, Rodrigues JM, Queiroz MJRP, Calhelha RC, Ferreira ICFR et al (2021) Magnetoliposomes based on magnetic/plasmonic nanoparticles loaded with tricyclic lactones for combined cancer therapy. Pharmaceutics 13:1905. https://doi.org/10.3390/PHARMACEUTICS13111905/S1
16. Manickam V, Periyasamy M, Dhakshinamoorthy V, Panneerselvam L, Perumal E (2017) Recurrent exposure to ferric oxide nanoparticles alters myocardial oxidative stress, apoptosis and necrotic markers in male mice. Chem Biol Interact 278:54–64. https://doi.org/10.1016/j.cbi.2017.10.003
17. Yousef M, Abuzreda A, Kamel M (2019) Cardiotoxicity and lung toxicity in male rats induced by long-term exposure to iron oxide and silver nanoparticles. Exp Ther Med. https://doi.org/10.3892/etm.2019.8108
18. Qualhato G, Rocha TL, de Oliveira Lima EC, e Silva DM, Cardoso JR, Koppe Grisolia C et al (2017) Genotoxic and mutagenic assessment of iron oxide (maghemite-g-Fe_2O_3) nanoparticle in the guppy *Poecilia reticulata*. Chemosphere 183:305–314. https://doi.org/10.1016/J.CHEMOSPHERE.2017.05.061
19. Sieber S, Grossen P, Bussmann J, Campbell F, Kros A, Witzigmann D et al (2019) Zebrafish as a preclinical in vivo screening model for nanomedicines. Adv Drug Deliv Rev 151–152:152–168. https://doi.org/10.1016/j.addr.2019.01.001
20. Caro C, Egea-Benavente D, Polvillo R, Royo JL, Pernia Leal M, García-Martín ML (2019) Comprehensive toxicity assessment of PEGylated magnetic nanoparticles for in vivo applications. Colloids Surf B Biointerfaces 177:253–259. https://doi.org/10.1016/j.colsurfb.2019.01.051
21. Howe K, Clark MD, Torroja CF, Torrance J, Berthelot C, Muffato M et al (2013) The zebrafish reference genome sequence and its relationship to the human genome. Nature 496:498–503. https://doi.org/10.1038/nature12111
22. Brito RS, Canedo A, Farias D, Rocha TL (2022) Transgenic zebrafish (*Danio rerio*) as an emerging model system in ecotoxicology and toxicology: historical review, recent advances, and trends. Sci Total Environ 848:157665. https://doi.org/10.1016/j.scitotenv.2022.157665
23. White R, Rose K, Zon L (2013) Zebrafish cancer: the state of the art and the path forward. Nat Rev Cancer 13(9):624–636. https://doi.org/10.1038/nrc3589
24. Jacintho JC, Ferreira ACN, Rocha TL (2025) Zebrafish as a model for assessing the nanotechnology-based approaches in cancer diagnosis, therapy and theranostic: a historical review, trends and challenges. Nanomedicine 70:102867. https://doi.org/10.1016/J.NANO.2025.102867
25. OECD (2013) Test No. 236: Fish Embryo Acute Toxicity (FET) Test. OECD Guidelines for the Testing of Chemicals, Section "Materials and methods", OECD Publishing, pp 1–22
26. Pereira AC, Gomes T, Ferreira Machado MR, Rocha TL (2019) The zebrafish embryotoxicity test (ZET) for nanotoxicity assessment: from morphological to molecular approach. Environ Pollut 252:1841–1853. https://doi.org/10.1016/j.envpol.2019.06.100
27. Lin S, Zhao Y, Xia T, Meng H, Ji Z, Liu R et al (2011) High content screening in zebrafish speeds up hazard ranking of transition metal oxide nanoparticles. ACS Nano 5:7284–7295. https://doi.org/10.1021/nn202116p
28. Lin S, Lin S, Zhao Y, Nel AE (2013) Zebrafish: an in vivo model for nano EHS studies. Small 9:1608–1618. https://doi.org/10.1002/SMLL.201202115
29. Pereira AC, Gonçalves BB, Brito RdaS, Vieira LG, Lima ECdeO, Rocha TL (2020) Comparative developmental toxicity of iron oxide nanoparticles and ferric chloride to zebrafish (*Danio rerio*) after static and semi-static exposure. Chemosphere. https://doi.org/10.1016/j.chemosphere.2020.126792
30. Oliveira EMN, Selli GI, von Schmude A, Miguel C, Laurent S, Vianna MRM et al (2020) Developmental toxicity of iron oxide nanoparticles with different coatings in zebrafish larvae. J Nanopart Res 22:1–16. https://doi.org/10.1007/s11051-020-04800-2
31. Thirumurthi NA, Raghunath A, Balasubramanian S, Perumal E (2022) Evaluation of maghemite nanoparticles-induced developmental toxicity and oxidative stress in zebrafish embryos/larvae. Biol Trace Elem Res 200:2349–2364. https://doi.org/10.1007/S12011-021-02830-Y
32. Sheel R, Kumari P, Panda PK, Jawed Ansari MD, Patel P, Singh S et al (2020) Molecular intrinsic proximal interaction infer oxidative stress and apoptosis modulated *in vivo* biocompatibility of *P.niruri* contrived antibacterial iron oxide nanoparticles with zebrafish. Environ Pollut 267:115482. https://doi.org/10.1016/j.envpol.2020.115482
33. Sousa ACC, Romo AIB, Almeida RR, Silva ACC, Fechine LMU, Brito DHA et al (2021) Starch-based magnetic nanocomposite for targeted delivery of hydrophilic bioactives as anticancer strategy. Carbohydr Polym. https://doi.org/10.1016/J.CARBPOL.2021.118017

34. Chandrasekaran K, Chung SM (2025) Bio-functional Mn_2O_3-carboxymethyl cellulose-L-arginine hybrid nanomaterials for targeting *Candida albicans* and oral cancer. Int J Biol Macromol 320:145782. https://doi.org/10.1016/J.IJBIOMAC.2025.145782
35. Suganya D, Ramakritinan CM, Rajan MR (2018) Adverse effects of genotoxicity, bioaccumulation and ionoregulatory modulation of two differently synthesized iron oxide nanoparticles on zebrafish (*Danio rerio*). J Inorg Organomet Polym Mater 28:2603–2611. https://doi.org/10.1007/s10904-018-0935-3
36. Aquino VRR, Vinícius-Araújo M, Shrivastava N, Sousa MH, Coaquira JAH, Bakuzis AF (2019) Role of the fraction of blocked nanoparticles on the hyperthermia efficiency of Mn-based ferrites at clinically relevant conditions. J Phys Chem C. https://doi.org/10.1021/acs.jpcc.9b06599
37. Rodrigues HF, Mello FM, Branquinho LC, Zufelato N, Silveira-Lacerda EP, Bakuzis AF (2013) Real-time infrared thermography detection of magnetic nanoparticle hyperthermia in a murine model under a non-uniform field configuration. Int J Hyperthermia 29:752–767. https://doi.org/10.3109/02656736.2013.839056
38. ISO (1996) ISO 7346–3:1996 - Water quality - Determination of the acute lethal toxicity of substances to a freshwater fish [*Brachydanio rerio* Hamilton-Buchanan (Teleostei, Cyprinidae)] - Part 3: Flow-through method
39. Sajid MU, Bicer Y (2022) Impacts of ultrasonication time and surfactants on stability and optical properties of CuO, Fe3O4, and CNTs/water nanofluids for spectrum selective applications. Ultrason Sonochem 88:106079. https://doi.org/10.1016/j.ultsonch.2022.106079
40. Kimmel CB, Ballard WW, Kimmel SR, Ullmann B, Schilling TF (1995) Stages of embryonic development of the zebrafish. Dev Dyn 203:253–310. https://doi.org/10.1002/aja.1002030302
41. Ivask A, Titma T, Visnapuu M, Vija H, Kakinen A, Sihtmae M et al (2015) Toxicity of 11 metal oxide nanoparticles to three mammalian cell types in vitro. Curr Top Med Chem 15:1914–1929. https://doi.org/10.2174/1568026615666150506150109
42. CONAMA Resolution n. 430/2011 Brazil - Federal - LegisWeb n.d. https://www.legisweb.com.br/legislacao/?id=114770 . Accessed 25 July 2025
43. Ates M, Demir V, Arslan Z, Kaya H, Yilmaz S, Camas M (2016) Chronic exposure of tilapia (*Oreochromis niloticus*) to iron oxide nanoparticles: effects of particle morphology on accumulation, elimination, hematology and immune responses. Aquat Toxicol 177:22–32. https://doi.org/10.1016/J.AQUATOX.2016.05.005
44. Lammer E, Carr GJ, Wendler K, Rawlings JM, Belanger SE, Braunbeck T (2009) Is the fish embryo toxicity test (FET) with the zebrafish (*Danio rerio*) a potential alternative for the fish acute toxicity test? Comp Biochem Physiol C Toxicol Pharmacol 149:196–209. https://doi.org/10.1016/j.cbpc.2008.11.006
45. Krzykwa JC, Saeid A, Jeffries MKS (2019) Identifying sublethal endpoints for evaluating neurotoxic compounds utilizing the fish embryo toxicity test. Ecotoxicol Environ Saf 170:521–529. https://doi.org/10.1016/j.ecoenv.2018.11.118
46. Babić S, Barišić J, Višić H, Sauerborn Klobučar R, Topić Popović N, Strunjak-Perović I et al (2017) Embryotoxic and genotoxic effects of sewage effluents in zebrafish embryo using multiple endpoint testing. Water Res 115:9–21. https://doi.org/10.1016/J.WATRES.2017.02.049
47. Pitombeira de Figueirêdo L, Cirqueira F, de Sousa BLC, Mamboungou J, Rocha TL (2025) Developmental toxicity of formulated insecticide mixture containing imidacloprid and beta-cyfluthrin in fish: insights using zebrafish. Chemosphere 377:144314. https://doi.org/10.1016/j.chemosphere.2025.144314
48. Zhao X, Wang S, Wu Y, You H, Lv L (2013) Acute ZnO nanoparticles exposure induces developmental toxicity, oxidative stress and DNA damage in embryo-larval zebrafish. Aquat Toxicol 136–137:49–59. https://doi.org/10.1016/J.AQUATOX.2013.03.019
49. Muthulakshmi S, Maharajan K, Habibi HR, Kadirvelu K, Venkataramana M (2018) Zearalenone induced embryo and neurotoxicity in zebrafish model (*Danio rerio*): role of oxidative stress revealed by a multi biomarker study. Chemosphere 198:111–121. https://doi.org/10.1016/J.CHEMOSPHERE.2018.01.141
50. Bradford MM (1976) A rapid and sensitive method for the quantitation of microgram quantities of protein utilizing the principle of protein-dye binding. Anal Biochem 72:248–254. https://doi.org/10.1016/0003-2697(76)90527-3
51. Zhao W, Hu N, Ding D, Long D, Li S, Li G et al (2019) Developmental toxicity and apoptosis in zebrafish embryos induced by low-dose γ-ray irradiation. Environ Sci Pollut Res 26:3869–3881. https://doi.org/10.1007/S11356-018-3893-Y/METRICS
52. Qualhato G, Cirqueira Dias F, Rocha TL (2024) Hazardous effects of plastic microfibres from facial masks to aquatic animal health: insights from zebrafish model. Sci Total Environ 951:175555. https://doi.org/10.1016/J.SCITOTENV.2024.175555
53. Lin Y, Yu J, Wang M, Wu L (2023) Toxicity of single and combined 4-epianhydrotetracycline and cadmium at environmentally relevant concentrations on the zebrafish embryos (*Danio rerio*). Environ Pollut 316:120543. https://doi.org/10.1016/J.ENVPOL.2022.120543
54. Pinheiro-da-Silva J, Silva PF, Nogueira MB, Luchiari AC (2017) Sleep deprivation effects on object discrimination task in zebrafish (*Danio rerio*). Anim Cogn 20:159–169. https://doi.org/10.1007/s10071-016-1034-x
55. Santos AL, Rodrigues LC, Rodrigues CC, Cirqueira F, Malafaia G, Rocha TL (2024) Polystyrene nanoplastics induce developmental impairments and vasotoxicity in zebrafish (*Danio rerio*). J Hazard Mater. https://doi.org/10.1016/j.jhazmat.2023.132880
56. Tang ZX, Sorensen CM, Klabunde KJ, Hadjipanayis GC (1991) Size-dependent Curie temperature in nanoscale $MnFe_2O_4$ particles. Phys Rev Lett 67:3602–3605. https://doi.org/10.1103/PhysRevLett.67.3602

57. Lunardi CN, Gomes AJ, Rocha FS, De Tommaso J, Patience GS (2021) Experimental methods in chemical engineering: zeta potential. Can J Chem Eng 99:627–639. https://doi.org/10.1002/CJCE.23914
58. Ovanesyan Z, Aljzmi A, Almusaynid M, Khan A, Valderrama E, Nash KL et al (2015) Ion-ion correlation, solvent excluded volume and pH effects on physicochemical properties of spherical oxide nanoparticles. J Colloid Interface Sci 462:325. https://doi.org/10.1016/J.JCIS.2015.10.019
59. Lundin L, Keiter SH (2025) Zebrafish as a model to investigate nanoparticles. nanosafety: a comprehensive approach to assess nanomaterial exposure on the environment and health, pp 365–400. https://doi.org/10.1007/978-3-031-93871-9_14
60. Chao SJ, Huang CP, Chen PC, Chang SH, Huang C (2018) Uptake of BDE-209 on zebrafish embryos as affected by SiO_2 nanoparticles. Chemosphere 205:570–578. https://doi.org/10.1016/J.CHEMOSPHERE.2018.04.075
61. Nagaraj A, Ghosh OSN, Ghneim HK, AlSheikh YA, Mohammed K, Poda S et al (2025) Fe_2O_3-type iron oxide nanoparticles from *Aerva lanata* leaf extract exhibit antibiofilm, discriminatory toxicity in cancer cells, and theranostic against oxidative stress in zebrafish. ChemPhys Impact 10:100849. https://doi.org/10.1016/J.CHPHI.2025.100849
62. Gowtham P, Girigoswami K, Prabhu AD, Pallavi P, Thirumalai A, Harini K et al (2024) Hydrogels of Alginate derivative-encased nanodots featuring carbon-coated Manganese Ferrite cores with Gold shells to offer antiangiogenesis with multimodal imaging-based theranostics. Adv Ther 7:2400054. https://doi.org/10.1002/ADTP.202400054
63. Karunakaran G, Cho EB, Thirumurugan K, Kumar GS, Kolesnikov E, Boobalan S et al (2021) Mesoporous Mn-doped hydroxyapatite nanorods obtained via pyridinium chloride enabled microwave-assisted synthesis by utilizing *Donax variabilis* seashells for implant applications. Mater Sci Eng, C 126:112170. https://doi.org/10.1016/J.MSEC.2021.112170
64. Lyu Z, Kou Y, Fu Y, Xie Y, Yang B, Zhu H et al (2024) Comparative transcriptomics revealed neurodevelopmental impairments and ferroptosis induced by extremely small iron oxide nanoparticles. Front Genet. https://doi.org/10.3389/fgene.2024.1402771
65. Baker C, Hasanain SK, Shah SI (2004) The magnetic behavior of iron oxide passivated iron nanoparticles. J Appl Phys 96:6657–6662. https://doi.org/10.1063/1.1806263
66. Rawson DM, Zhang T, Kalicharan D, Jongebloed WL (2000) Field emission scanning electron microscopy and transmission electron microscopy studies of the chorion, plasma membrane and syncytial layers of the gastrula-stage embryo of the zebrafish *Brachydanio rerio*: a consideration of the structural and functional relationships with respect to cryoprotectant penetration. Aquac Res 31:325–336. https://doi.org/10.1046/J.1365-2109.2000.00401.X
67. da Silva GH, Clemente Z, Khan LU, Coa F, Neto LLR, Carvalho HWP et al (2018) Toxicity assessment of TiO2-MWCNT nanohybrid material with enhanced photocatalytic activity on *Danio rerio* (zebrafish) embryos. Ecotoxicol Environ Saf 165:136–143. https://doi.org/10.1016/J.ECOENV.2018.08.093
68. Son JH, Gerenza AK, Bingener GM, Bonkowsky JL (2022) Hypoplasia of dopaminergic neurons by hypoxia-induced neurotoxicity is associated with disrupted swimming development of larval zebrafish. Front Cell Neurosci 16:963037. https://doi.org/10.3389/fncel.2022.963037
69. Burkitt MJ, Gilbert BC (1991) The autoxidation of iron(II) in aqueous systems: the effects of iron chelation by physiological, non-physiological and therapeutic chelators on the generation of reactive oxygen species and the inducement of biomolecular damage. Free Radic Res Commun 14:107–123. https://doi.org/10.3109/10715769109094123
70. Wu L, Wen W, Wang X, Huang D, Cao J, Qi X et al (2022) Ultrasmall iron oxide nanoparticles cause significant toxicity by specifically inducing acute oxidative stress to multiple organs. Part Fibre Toxicol 19:1–14. https://doi.org/10.1186/s12989-022-00465-y
71. Wang D, Lin Z, Wang T, Yao Z, Qin M, Zheng S et al (2016) Where does the toxicity of metal oxide nanoparticles come from: the nanoparticles, the ions, or a combination of both? J Hazard Mater 308:328–334. https://doi.org/10.1016/J.JHAZMAT.2016.01.066
72. Zhu X, Tian S, Cai Z (2012) Toxicity assessment of iron oxide nanoparticles in zebrafish (*Danio rerio*) early life stages. PLoS ONE 7:e46286. https://doi.org/10.1371/JOURNAL.PONE.0046286
73. Olayinka O, Ryu H, Wang X, Malik AB, Jung HM (2025) Compensatory lymphangiogenesis is required for edema resolution in zebrafish. Sci Rep. https://doi.org/10.1038/S41598-025-92970-1
74. Huang B-X, Zhang T, Dong Q-B, Lin P-X, Zhou Y, Chen X-S (2026) Neurodevelopmental toxicity induced by iron oxide nanoparticles: insights from chick and zebrafish embryonic models. Comp Biochem Physiol C Toxicol Pharmacol 299:110372. https://doi.org/10.1016/J.CBPC.2025.110372
75. Iversen NK, Frische S, Thomsen K, Laustsen C, Pedersen M, Hansen PBL et al (2013) Superparamagnetic iron oxide polyacrylic acid coated γ-Fe2O3 nanoparticles do not affect kidney function but cause acute effect on the cardiovascular function in healthy mice. Toxicol Appl Pharmacol 266:276–288. https://doi.org/10.1016/j.taap.2012.10.014
76. Nunes ADC, Ramalho LS, Souza ÁPS, Mendes EP, Colugnati DB, Zufelato N et al (2014) Manganese ferrite-based nanoparticles induce ex vivo, but not in vivo, cardiovascular effects. Int J Nanomedicine 9:3299–3312. https://doi.org/10.2147/IJN.S64254

77. Nunes ADC, Gomes-Silva LA, Zufelato N, Prospero AG, Quini CC, Matos RVR et al (2019) Albumin coating prevents cardiac effect of the magnetic nanoparticles. IEEE Trans Nanobiosci 18:640–650. https://doi.org/10.1109/TNB.2019.2931962
78. Mohammadi MR, Malkovskiy AV, Jothimuthu P, Kim KM, Parekh M, Inayathullah M et al (2018) PEG/Dextran double layer influences Fe ion release and colloidal stability of iron oxide nanoparticles. Sci Rep. https://doi.org/10.1038/S41598-018-22644-8
79. Zhou C, Wu F, He L, Yan H, Zhang Z, Zhao S et al (2025) An implant-free nanosystem enabling synergistic oxidative damage mitigation and deep brain stimulation for alleviating Parkinsonian symptoms. ACS Nano 19:26715–26734. https://doi.org/10.1021/acsnano.5c06227
80. Worley CG, Bombick D, Allen JW, Lee Suber R, Aschner M (2002) Effects of manganese on oxidative stress in CATH.a cells. Neurotoxicology 23:159–164. https://doi.org/10.1016/S0161-813X(02)00028-1
81. Fang YY, Teng MJ, Peng JC, Zheng XW, Mo YQ, Ho TT et al (2024) Combined exposure to manganese and iron decreases oxidative stress-induced nerve damage by increasing Nrf2/HO-1/NQO1 expression. Ecotoxicol Environ Saf 270:115853. https://doi.org/10.1016/J.ECOENV.2023.115853
82. Hussain SM, Javorina AK, Schrand AM, Duhart HMHM, Ali SF, Schlager JJ (2006) The interaction of manganese nanoparticles with PC-12 cells induces dopamine depletion. Toxicol Sci 92:456–463. https://doi.org/10.1093/TOXSCI/KFL020
83. Araújo PS, Caixeta MB, Qualhato G, Gonçalves BB, Gomes RS, Viali da SN E et al (2025) Genotoxicity, mutagenicity, and immunotoxicity assessment of green silver nanoparticles from *Croton urucurana* on neotropical snails *Biomphalaria glabrata*. Environ Pollut 377:126424. https://doi.org/10.1016/J.ENVPOL.2025.126424